

# X-ray and Gamma-ray Emissions from Rotation Powered Millisecond Pulsars

J. Takata<sup>1</sup>

takata@hku.hk

K. S. Cheng<sup>1</sup>

hrspksc@hkucc.hku.hk

and

Ronald E. Taam<sup>2,3</sup>

r-taam@northwestern.edu

## ABSTRACT

The *Fermi*-LAT has revealed that rotation powered millisecond pulsars (MSPs) are a major contributor to the Galactic  $\gamma$ -ray source population. Such pulsars may also be important in modeling the quiescent state of several low mass X-ray binaries (LMXBs), where optical observations of the companion star suggest the possible existence of rotation powered MSPs. To understand the observational properties of the different evolutionary stages of MSPs, the X-ray and  $\gamma$ -ray emission associated with the outer gap model is investigated. For rotation powered MSPs, the size of the outer gap and the properties of the high-energy emission are controlled by either the photon-photon pair-creation process or magnetic pair-creation process near the surface. For these pulsars, we find that the outer gap model controlled by the magnetic pair-creation process is preferable in explaining the possible correlations between the  $\gamma$ -ray luminosity or non-thermal X-ray luminosity versus the spin down power. For the accreting MSPs in quiescent LMXBs, the thermal X-ray emission at the neutron star surface resulting from deep crustal heating can control the conditions in the outer gap. We argue that the optical modulation observed in the quiescent state of several LMXBs

---

<sup>1</sup>Department of Physics, University of Hong Kong, Pokfulam Road, Hong Kong

<sup>2</sup>Department of Physics and Astronomy, Northwestern University, 2131 Tech Drive, Evanston, IL 60208

<sup>3</sup>Academia Sinica Institute of Astronomy and Astrophysics - TIARA, P.O. Box 23-141, Taipei, 10617 Taiwan

originates from the irradiation of the donor star by  $\gamma$ -rays from the outer gap. In these systems, the irradiation luminosity required for the optical modulation of the source such as SAX J1808.4-3658 can be achieved for a neutron star of high mass. Finally, we discuss the high-energy emission associated with an intra-binary shock in black widow systems, e.g. PSR B1957+20.

*Subject headings:* binaries: close; — magnetic fields: pulsars; — stars: neutron

## 1. Introduction

The *Fermi* Large Area Telescope (*Fermi*-LAT) has discovered over 80  $\gamma$ -ray pulsars, and revealed that the  $\gamma$ -ray pulsars are a major class of Galactic  $\gamma$ -ray sources. Of these, *Fermi*-LAT first detected pulsed  $\gamma$ -ray emission from 11 millisecond pulsars, hereafter denoted as MSPs (Abdo et al. 2010a,b,c, 2009a,b; Saz Parkinson et al. 2010; Guillemot et al. 2011). The  $\gamma$ -ray emission from pulsars has a long history, having been discussed in the context of a polar cap accelerator (Ruderman & Sutherland 1975; Daugherty & Harding 1982, 1996), a slot gap (Arons 1983; Muslimov & Harding 2004; Harding, Usov & Muslimov 2005; Harding et al. 2008; Harding & Muslimov 2011) and an outer gap accelerator (Cheng, Ho & Ruderman 1986a,b; Hirotani 2008; Takata, Wang & Cheng 2010b). The cut-off features of the  $\gamma$ -ray spectra of the Crab and the Vela pulsars as measured by *Fermi* imply that the  $\gamma$ -ray emission site of canonical pulsars is located in the outer magnetosphere. This is in contrast to a site near the polar cap region which produces a cut-off feature steeper than observed (Aliu et al. 2009; Abdo et al. 2009c, 2010d). However, Venter, Harding & Guillemot (2009) found that the observed pulse profiles of several MSPs detected by the *Fermi* cannot be explained by the outer gap and/or the slot gap models. Hence, they proposed a pair-starved polar cap model in which particles are continuously accelerated to high altitude because multiplicity of the pairs is insufficient to screen the electric field. Therefore, the origin of the  $\gamma$ -ray emission from MSPs remains to be clarified.

We present the spin period vs. the dipole moment for the rotation powered MSPs in Figure 1, in which the  $\gamma$ -ray emitting MSPs are marked with open circles. The spin period in the accretion stage may be related to the equilibrium spin period, which is obtained by equating the co-rotation radius  $r_{co} = (GMP^2/4\pi^2)^{1/3}$  to the Alfvén radius  $r_M = (\mu^4/2GM\dot{M})^{1/7}$ , where  $M$  is the neutron star mass and  $\dot{M}$  is the accretion rate. The equilibrium spin period implies  $\mu \propto P^{7/6}$  (Alpar et al. 1982). In Figure 1, we illustrate the relation  $\mu_{26} = \kappa P_{-3}^{7/6}$ , where  $P_{-3} = (P/1 \text{ ms})$ ,  $\mu_{26} = (\mu/10^{26} \text{ G cm}^3)$ . The normalization factor is chosen as  $\kappa = 1.5$  (solid line), which gives an upper limit to the magnetic field for the recently activated radio MSP PSR J1023+0038 (see below), and  $\kappa = 1/3$  (dash line), which reproduces the typical

$P - \mu$  relation for the Fermi-LAT MSPs and the radio MSPs. In section 4, we apply the above relations to estimate the magnetic moment of accreting MSPs.

In Figure 1, the new radio MSPs, whose locations are coincident with the *Fermi* unidentified sources are marked with boxes. In fact, it has been pointed out that over 20 new radio MSPs have been discovered as *Fermi* identified sources (e.g. Keith et al. 2011). Since the detection of the spin period of MSPs (in particular in binary systems) via a blind search is very difficult, it is likely that *Fermi* has missed the identification of many MSPs. Thus, some of them may be associated with the *Fermi* unidentified sources. For example, Takata, Wang and Cheng (2011a,b,c) performed population studies of  $\gamma$ -ray pulsars and argued on statistical grounds that the  $\gamma$ -ray emission from over 100 MSPs are missed, possibly contributing to the *Fermi* unidentified sources.

PSR J1023+0038 is known to be the first and only rotation powered radio MSP in a quiescent low-mass X-ray binary (LMXB) FIRST J102347.67+003841.2. The possibility of  $\gamma$ -ray emission from the newly born MSP PSR J1023+0038 has been pointed out by Tam et al. (2010). This system showed clear evidence of an accretion disk in 2001 and its possible absence in 2002 (Wang et al. 2009), perhaps indicating that the pulsar became activated. To facilitate the transition from an accreting MSP X-ray pulsars (AMP) to a rotation powered MSP, the accretion of matter onto the NS must decrease rapidly. Campana et al. (1998) argued that the “propeller” effect, in which the Alfvén radius exceeds the co-rotation radius, operates during the quiescent state of an X-ray transient LMXB phase (Romanova et al. 2009) to eject matter from the system. Takata, Cheng & Taam (2010a) suggest that the activation of the rotation powered pulsar phase in a short period LMXB is likely to occur during the quiescent state and that the  $\gamma$ -ray emission produced in the outer gap accelerator in the pulsar magnetosphere irradiates the surrounding disk, thereby, further enhancing this ejection of disk material.

The activation of rotation powered pulsars has been hypothesized based on the orbital modulations in the optical emission observed in the quiescent state of LMXBs, i.e., First 102347.68+003841.2 (Thorstensen & Armstrong 2005), SAX J1808.4-3658 (Burderi et al. 2003; Deloye et al. 2008), XTE 1814-338 (D’Avanzo et al. 2009), and IGR J00291+5934 (Jonker et al. 2008). In these systems, the amplitude of the optical modulation can not be explained by irradiation associated with the X-ray emission from the disk or from the neutron star (NS) surface due to insufficient luminosity. To provide an explanation of the orbital modulation of the optical emission, pulsar wind models have been suggested in which heating of the donor is due to the effect of a relativistic pulsar wind (Burderi et al. 2003). However there are some unresolved issues on this picture; for example, (1) heating process of the stellar matter by the pulsar magnetic field if the wind energy near the companion star

is dominated by the magnetic energy and (2) conversion mechanism from electromagnetic energy into the particle energy within  $r \sim 10^{10-11}$  cm from the pulsar if the wind energy is dominated by the particle energy. In this paper, because of the large theoretical uncertainties on the pulsar wind model, we will not pursue this picture in further detail. Alternatively, we will discuss the  $\gamma$ -ray irradiation from the outer gap as a possible heating process of the companion star (section 4).

In the X-ray band, the emission from rotation powered MSPs can be composed of thermal emission from a heated polar cap region plus (for some pulsars) non-thermal emission of magnetospheric origin. Although the number of the non-thermal X-ray emitting MSPs have increased due to the improved sensitivity of recent X-ray instruments (e.g. Zavlin 2007), the origin of pulsed non-thermal X-ray emission from MSPs is not well understood. Since the population of the  $\gamma$ -ray MSPs has increased due to the detections by the *Fermi*-LAT, a study of the emission process in the X-ray and  $\gamma$ -ray bands is necessary for discriminating between various non-thermal emission processes in the magnetosphere.

Observationally, X-ray emission from the NS surface has been detected during the quiescent state of several LMXBs (see Heinke et al. 2009 and reference therein). This emission coupled with estimates for the time averaged mass accretion rate has been utilized to probe the equation of state of NS matter (e.g. Yakovlev, Levenfish & Haensel 2003; Campana et al. 2008). For some systems, the thermal X-ray emission may be very weak in the quiescent state (e.g., SAX J1808.4-3658) and the X-ray emission may be well fit by a power law spectrum (Heinke et al. 2009). The finding of non-thermal X-ray emission from SAX J1808.4-3658 may provide possible evidence for the activation of the rotation powered activity in the quiescent state, although the origin of this power law component is unclear at present, as it may be due, for example, to the emission from the magnetosphere or intra-binary shock.

The X-ray emission from an intra-binary shock in the MSP and low mass star (hereafter LMS) system has been suggested to explain the observed unresolved non-thermal X-ray emissions from PSR B1957/LMS binary system (Arons & Tavani 1993; Stappers et al. 2003; Huang & Becker 2007), in which the LMS eclipses the radio emission from the MSP. Moreover, similar binary (so called “black widow”) systems have been discovered at the positions of the *Fermi* unidentified sources (Roberts et al. 2011), which raises questions regarding the origin of the high-energy emissions from MSP/LMS system.

As we have described above, observational evidence for non-thermal X-ray and  $\gamma$ -ray emission from the different evolutionary stages of MSPs has been accumulating. In this paper, we discuss the  $\gamma$ -ray and X-ray emissions from isolated rotation powered MSPs and those in binary systems. Specifically, we model the  $\gamma$ -ray emission from the outer gap of the MSPs, and explore (1) the origin of the  $\gamma$ -ray emission from rotation powered MSPs detected

by *Fermi*-LAT and (2) the possibility that irradiation by the  $\gamma$ -rays from the outer gap can explain the optical modulation of quiescent LMXBs. We also discuss the non-thermal X-ray emission associated with the outer gap activities and the high-energy emission from an intra-binary shock. In section 2, we review the  $\gamma$ -ray emission from the outer gap accelerator in a pulsar magnetosphere and suggest that the thermal X-ray emission from the polar cap region can arise from the heating due to incoming particles, which were accelerated in the outer gap. In section 3, we apply the model to the rotation powered MSPs and compare the predicted  $\gamma$ -ray luminosity with the *Fermi* observations. In section 4, the various processes determining the NS surface temperature which depend on the NS model of the accreting millisecond pulsars (AMPs) in quiescent LMXBs are discussed. In addition, we estimate the  $\gamma$ -ray luminosity from the outer gap accelerator. In section 5, the non-thermal X-ray emission is discussed within the context of the outer gap model, and we predict the relation between the non-thermal X-ray luminosity and the spin down power of rotation powered MSPs. In addition, the non-thermal X-ray luminosity from the AMP in the quiescent LMXB is discussed as a function of the time averaged accretion rate. In section 6, we discuss high-energy emission from an intra-binary shock in MSP/LMXB binary, and describe the difference in the properties between the intra-binary shock emission and the magnetospheric emission. Finally, a brief summary is presented in the last section.

## 2. X-ray and $\gamma$ -ray radiation processes

### 2.1. $\gamma$ -ray emissions from the outer gap

In the outer gap accelerator model for rotation powered pulsars, electrons and/or positrons can be accelerated by the electric field along the magnetic field lines in the region where the local charge density deviates from the Goldreich-Julian charge density. The typical strength of the accelerating field in the gap is expressed as (Zhang & Cheng 1997)

$$E_{||} \sim \frac{f^2 V_a}{s} \sim 9 \times 10^5 f^2 \left( \frac{P}{10^{-3} \text{ s}} \right)^{-3} \left( \frac{\mu}{10^{26} \text{ G cm}^3} \right) \left( \frac{s}{R_{lc}} \right)^{-1} \text{ (c.g.s.)}, \quad (1)$$

where  $V_a = \mu/R_{lc}^2$  is the electrical potential drop across the polar cap,  $P$  is the spin period,  $\mu$  is the dipole moment of the NS,  $s$  is the curvature radius of the magnetic field line and  $R_{lc} = cP/2\pi$  is the light cylinder radius. In addition,  $f$  is the fractional gap thickness, which is defined as the ratio of the gap thickness at the light cylinder to the light cylinder radius  $R_{lc}$ . From the energy balance between the dipole radiation and the spin down of the pulsar, the dipole moment of the NS is estimated from

$$\mu \sim \sqrt{3\pi} I^{1/2} R_{lc}^{3/2} P^{-1} \dot{P}^{1/2} \sim 3 \times 10^{26} \sqrt{P_{-3} \dot{P}_{-19}} \text{ G cm}^3 \quad (2)$$

where  $I$  is NS moment of inertia assumed to be  $I = 10^{45} \text{ g cm}^2$ . In addition,  $\dot{P}_{-19}$  is the time derivative of the spin period in units of  $10^{-19} \text{ s/s}$ .

By assuming force balance between the acceleration and radiation reaction of the curvature radiation process, the typical Lorentz factor of the particles in the gap is

$$\Gamma = \left( \frac{3s^2}{2e} E_{\parallel} \right)^{1/4} \sim 2 \times 10^7 f^{1/2} P_{-3}^{-1/4} \mu_{26}^{1/4} s_*^{1/4}, \quad (3)$$

where  $s_* = (s/R_{lc})$ . The typical energy of the curvature photons is estimated to be

$$E_c = \frac{3hc\Gamma^3}{4\pi s} \sim 25 f^{3/2} P_{-3}^{-7/4} \mu_{26}^{3/4} s_*^{-1/4} \text{ GeV}. \quad (4)$$

The  $\gamma$ -ray luminosity from the outer gap is typically

$$L_{\gamma} \sim f^3 L_{sd} = 3.8 \times 10^{35} f^3 P_{-3}^{-4} \mu_{26}^2 \text{ erg s}^{-1}, \quad (5)$$

where we used the spin down power  $L_{sd} = 2(2\pi)^4 \mu^2 / 3P^4 c^3$ .

We note that the electron and positron pairs are mainly created around the inner boundary of the outer gap (Cheng, Ruderman & Zhang 2000; Takata, Chang & Shibata 2008; Takata et al. 2010b), implying that the outgoing particles are accelerated with whole gap potential drop, whereas the incoming particles can only receive  $\leq 10\%$  of the gap potential drop. Hence, we expect that the power carried by the outgoing particles is, at least, one order of magnitude greater than that carried by the incoming particles. In the gap, furthermore, because the curvature radiation process is occurring under the force balance between the acceleration force and the radiation back reaction force, as assumed in equation (3), the particles lose most of the energy gain via the curvature radiation process. Hence, the luminosity of the outgoing  $\gamma$ -rays is, at least, one order of magnitude greater than that of the incoming  $\gamma$ -rays. As we will discuss in section 2.2, the incoming particles eventually reach the stellar surface and heat up the polar cap region, producing the observed thermal X-ray emissions. The Lorentz factor of the incoming particles is reduced from  $\sim 10^7$  at the inner boundary of the outer gap to  $\sim 8 \times 10^5$  at the stellar surface, indicating the X-ray emissions from the heated polar cap region is at least two order of magnitude less than the outgoing  $\gamma$ -rays radiated by the outgoing particles.

As equation (5) indicates, the  $\gamma$ -ray luminosity from the pulsar depends on its spin down luminosity. On the other hand, the spin down luminosity depends on the structure of magnetosphere and the inclination angle between the magnetic axis and the rotation axis, indicating the predicted  $\gamma$ -ray luminosity from the outer gap depends on the structure of the pulsar magnetosphere. For example, Spitkovsky (2006) represented the dipole field

structure in the ideal MHD limit, in which there is no accelerating field, and found that the inferred spin down luminosity,  $L_{sd}^{MHD} \sim (2\pi)^4 \mu^2 / (P^4 c^3) \times (1 + \sin^2 \theta_o^2)$ , can be up to 3 times larger than the standard vacuum formula  $L_{sd}^{va} \sim 2(2\pi)^4 \mu^2 / (3P^4 c^3)$ , where  $\theta_o$  is the inclination angle. Although the magnetospheric structure has not been understood well, the real magnetosphere with the accelerating region will be between the vacuum limit and the ideal MHD limit (e.g. Constantinos et al. 2011; Li, Spitkovsky & Tchekhovskoy, 2011; Wada and Shibata 2011), and therefore the spin down luminosity will be only a factor of 1-3 different from that of standard formula ( $L_{sd}^{va}$ ). Furthermore, the detailed structure of the magnetosphere, such as the magnetic field configurations, will be more important to the pulse profiles and the phase-resolved spectra, which are beyond the scope of this paper. In this paper, therefore, we apply the standard formula as a typical magnitude of the spin down power.

## 2.2. Heated polar cap by incoming current

Half of the particles accelerated in the outer gap will return to the polar cap region and heat the stellar surface. Several rotation powered MSPs exhibit thermal X-ray radiation characterized by a temperature of  $T \sim 10^6$  K (Zavlin 2007), which is much higher than  $T \sim 10^5$  K expected from the standard neutrino cooling scenario (Yakovlev & Pethick 2004 for the review). Furthermore, the size of the inferred emitting region corresponds to an effective radius of  $10^{4-5}$  cm, which is much smaller than the NS radius. For some MSPs the observed X-ray spectra can be fit by black body radiation with two components, that is, a “core” component described by a higher temperature ( $T_c > 10^6$  K), but smaller effective radius ( $R_c \sim 10^{3-4}$  cm), and a “rim” component with a lower temperature ( $T_r \sim 5 \times 10^5$  K) and larger effective radius ( $R_r \sim 10^5$  cm). The observed temperatures and the effective radii of the 11  $\gamma$ -ray emitting MSPs are summarized in Table 1. These observations provide indirect evidence for additional heating of the polar cap region.

It has been hypothesized that near the stellar surface, the magnetic field configuration is not dominated by a dipole field (Ruderman 1991; Chen, Ruderman & Zhu 1998). Higher order multipole field configurations are likely and the strength of these components can be 1-3 orders of magnitude greater than the global dipole field. The distance  $\delta R_{eq}$  from the star for which the local magnetic field is comparable to the dipole field is estimated from the relation

$$B_s \left( \frac{l + \delta R_{eq}}{l} \right)^{-3} = B_d \left( \frac{R_s + \delta R_{eq}}{R_s} \right)^{-3} \quad (6)$$

where  $B_s$  is the strength of the local magnetic field at the stellar surface,  $R_s$  is the stellar radius, and  $l \sim (1 - 3) \times 10^5$  cm is the thickness of the NS crust. With  $B_s = 10 - 1000 B_d$ ,



we find  $\delta R_{eq} \sim (1 - 3)R_s$ . We expect that because of the bending of the local magnetic field with a smaller curvature radius ( $\sim 10^{5-6}$  cm) than  $\sim 10^7$  cm of the dipole field, the curvature photons emitted between  $R_s < r < R_s + \delta R_{eq}$  will illuminate a wider area on the stellar surface than that connected to the outer gap via the global dipolar magnetic field lines.

In Figure 2, we illustrate this picture for the structure of the polar cap region. The incoming relativistic particles, which were accelerated in the gap, lose their energy via curvature radiation between the stellar surface and the inner boundary of the gap, and its Lorentz factor decreases to  $\Gamma \sim 2 \times 10^6 P_{-3}^{1/3}$  [equation (8)] near the stellar surface ( $r \sim 2R_s$ ). Near the stellar surface, the incoming particles emit  $\gamma$ -ray photons with an energy  $m_e c^2 / \alpha_f \sim 70$  MeV, where  $m_e c^2$  is the electron rest mass energy and  $\alpha_f$  is the fine structure constant (Wang et al. 1998; Takata et al. 2010b). These 70 – 100 MeV photons may be converted into pairs via the local magnetic field, whose strength may reach  $B \sim 10^{11}$  Gauss. The local magnetic field will bend the trajectory of the incoming particles so that the  $\sim 100$  MeV photons will illuminate and heat a significant part of the polar cap region. The incoming particles eventually impact on the stellar surface with a Lorentz factor  $\sim 8 \times 10^5$  [equation (9)], and their remaining energy will heat an area much smaller than the polar cap region. We expect that the former and latter components are observed as the rim and core components respectively. With a strong local magnetic field, the typical size of the core component is estimated as  $R_c \sim f R_p (B_d / B_s)^{1/2}$  where  $R_p$  is the size of the polar cap region of the dipole field. This yields  $R_c \sim 0.2(f/0.5)P_{-3}^{-1/2}$  km with  $B_s = 10^2 B_d$ , which is consistent with the observations; for example  $R_c \sim 0.4$  km for PSR J 0030+4051 (Table 1).

Between the NS star surface and the inner boundary of the gap, the evolution of the Lorentz factor is approximately described by

$$m_e c^3 \frac{d\Gamma}{dr} = \frac{2}{3} \frac{\Gamma^4 e^2 c}{s^2}. \quad (7)$$

Near the surface,  $s \sim \sqrt{r R_{ls}}$  provides a good approximation for the curvature radius of the dipole field. Assuming that  $\delta R_{eq} \sim R_s$  and the Lorentz factor at  $r = R_s + \delta R_{eq}$  is much smaller than that at the inner boundary of the gap, we obtain

$$\Gamma(R_s + \delta R_{eq}) \sim \Gamma_1 [\ln(r_0 / (R_s + \delta R_{eq}))]^{-1/3} \sim \Gamma_1, \quad (8)$$

where  $r_0$  is the radial distance to the inner boundary of the gap and

$$\Gamma_1 \equiv \left( \frac{R_{lc} m_e c^2}{2e^2} \right)^{1/3} \sim 2 \times 10^6 P_{-3}^{1/3}.$$

In the region between  $R_s < r < R_s + \delta R_{eq}$ , the trajectories of the particles are described by the local magnetic field lines, which have a curvature radius of  $\zeta \sim 10^6$  cm. In such a



case, the Lorentz factor of the particles at the stellar surface can be estimated from

$$\Gamma_s \sim \left( \frac{m_e c^2 \zeta}{2\pi e^2} \right)^{1/3} \sim 8 \times 10^5 \zeta_6^{1/3} \quad (9)$$

where  $\zeta_6 = \zeta/10^6$  cm. The X-ray luminosity and temperatures for the rim ( $L_{X,r}, T_r$ ) and core ( $L_{X,c}, T_c$ ) components are calculated from

$$L_r = (\Gamma_1 - \Gamma_s) \dot{N} m_e c^2, \quad T_r = \left( \frac{L_{X,r}}{4\pi R_r^2 \sigma_s} \right)^{1/4}, \quad (10)$$

and

$$L_c = \Gamma_s \dot{N} m_e c^2, \quad T_c = \left( \frac{L_{X,c}}{4\pi R_c^2 \sigma_s} \right)^{1/4}, \quad (11)$$

respectively, where  $\dot{N}$  is the number of incoming particles per unit time and  $\sigma_s$  is the Stefan-Boltzmann constant. In addition,  $R_r$  and  $R_c$  are the effective radii of the heated region of the rim and core components respectively.

Wang, Takata and Cheng (2010) fit the phase-averaged spectrum of  $\gamma$ -ray pulsars using the outer gap model and suggested that the averaged current density is about 50 % of the Goldreich-Julian value. Hence, we take the rate of the incoming particles as

$$\dot{N} = f \frac{c\mu}{2eR_{lc}^2}. \quad (12)$$

As a result, the X-ray luminosity of the rim and core components are described by

$$L_r = (\Gamma_1 - \Gamma_s) m_e c^2 \dot{N} \sim 10^{32} f P_{-3}^{-5/3} \mu_{26} Q \text{ erg s}^{-1}, \quad (13)$$

and

$$L_c = \Gamma_s m_e c^2 \dot{N} \sim 5 \times 10^{31} f P_{-3}^{-2} \mu_{26} \zeta_6^{1/3} \text{ erg s}^{-1}, \quad (14)$$

where  $Q = 1 - [(\zeta/\pi R_{lc})^{1/3}]$ . The temperature of the heated surface becomes

$$T_r \sim 2 \times 10^6 f^{1/4} P_{-3}^{-5/12} \mu_{26}^{1/4} R_{r,5}^{-1/2} Q^{1/4} \text{ K}, \quad (15)$$

and

$$T_c \sim 5 \times 10^6 f^{1/4} P_{-3}^{-1/2} \mu_{26}^{1/4} R_{c,4}^{-1/2} \zeta_6^{1/12} \text{ K}, \quad (16)$$

respectively, where  $R_{r,5} = R_r/(10^5 \text{ cm})$  and  $R_{c,4} = R_c/(10^4 \text{ cm})$ .

For the canonical pulsar, the core component is observed with a luminosity one or two order of magnitude fainter than that of the rim component; for example,  $L_c \sim 10^{30} \text{ erg s}^{-1}$  and  $L_r \sim 10^{32} \text{ erg s}^{-1}$  for the Geminga pulsar (Kargaltsev et al. 2005). Halpern & Ruderman

(1993) studied the thermal X-ray emissions from the heated polar cap due to the bombardment of the incoming particles, which were accelerated in the outer gap, and found that the predicted luminosity  $\sim 10^{32}$  erg s $^{-1}$  with a temperature  $T > 10^6$  K for the Geminga pulsar is too bright compared with the observed luminosity of the core component  $L_c \sim 10^{30}$  ergs $^{-1}$ . Hence, they proposed that most of the X-ray photons from the heated polar cap region is scattered by the resonant Compton scattering and are eventually redistributed as a thermal emission from almost entire surface with a temperature  $T < 10^6$  K, which is observed as the rim component (Wang et al. 1998; Cheng & Zhang 1999).

For the MSPs, the observed luminosity of the core component ( $L_c \sim 10^{31}$  erg s $^{-1}$ ) is comparable to that of the rim component ( $L_r$ ), as Table 1 indicates. In fact, our model predicts that most of thermal emissions from the heated polar cap regions directly emerge without the resonant scattering (section 3). Because of the weaker magnetic field of the MSPs, the resonant Compton scattering may be less effective as compared with the case of the canonical pulsar.

### 3. Application to the Rotation Powered Millisecond Pulsars

As argued by Takata et al. (2010b) the outer gap can be controlled by either the photon-photon pair-creation process or the magnetic pair-creation process. In this section, we first review the outer gap model controlled by the photon-photon pair-creation process in section 3.1 and the magnetic pair-creation process in section 3.2. For reference, Table 1 summarizes the observed parameters of the MSPs detected by the *Fermi*-LAT.

#### 3.1. Outer gap controlled by the photon-photon pair-creation process

The  $\gamma$ -rays emitted in the outer gap can collide with the X-rays from the heated polar cap and convert into electron-positron pairs. It is possible that this process, itself, controls the thickness of the outer gap (Zhang & Cheng 1997, 2003). However, given the existence of the rim and core components, it is not clear theoretically which component controls the outer gap. If both components illuminate the gap, the core component, which is of a higher temperature than the rim component, is more likely to control the size of the outer gap. On the other hand, with a small effective radius of  $R_c \sim 10^{3-4}$  cm, it is possible that the core component does not illuminate the outer gap. In this respect, the X-ray emission of the rim component, whose effective radius  $R_r \sim 10^{5-6}$  cm, has a greater likelihood of illuminating the outer gap. To avoid complexity in the theoretical argument, therefore, we only present

the case that thermal X-rays from the rim component control the size of the outer gap. We remark that if the  $\gamma$ -ray emission is controlled by the core component, the predicted  $\gamma$ -ray luminosity is several times smaller than presented here. However, the main conclusion in this paper will remain unchanged.

The use of the pair-creation condition  $E_\gamma E_X \sim (m_e c^2)^2$  together with equations (4) and (15) leads to the fractional gap thickness controlled by the photon-photon pair-creation process,  $f \equiv f_p$ , as

$$f_p \sim 0.1 P_{-3}^{26/21} \mu_{26}^{-4/7} s_*^{1/7} R_{r,5}^{2/7} Q^{-1/7}, \quad (17)$$

where the typical X-ray photon energy  $E_X = 3kT_r$  is used. The  $\gamma$ -ray luminosity (5) and the typical radiation energy (4) can be rewritten as

$$L_\gamma^p \sim 3.8 \times 10^{32} P_{-3}^{-2/7} \mu_{26}^{2/7} s_*^{3/7} R_{r,5}^{6/7} Q^{-3/7} \text{ erg s}^{-1}, \quad (18)$$

and

$$E_c^p \sim 0.8 P_{-3}^{3/28} \mu_{26}^{-3/28} s_*^{-1/28} R_{r,5}^{3/7} Q^{-3/14} \text{ GeV}. \quad (19)$$

The total X-ray luminosity  $L_X = L_r + L_c$  and the temperature of the heated surface are now given by

$$L_X^p \sim 10^{31} P_{-3}^{-3/7} \mu_{26}^{3/7} s_*^{1/7} R_{r,5}^{2/7} Q^{-1/7} \text{ erg s}^{-1}, \quad (20)$$

$$T_r^p \sim 10^6 P_{-3}^{-3/28} \mu_{26}^{3/28} s_*^{1/28} R_{r,5}^{-3/7} Q^{3/14} \text{ K}, \quad (21)$$

and

$$T_c^p \sim 3 \times 10^6 P_{-3}^{-4/21} \mu_{26}^{3/28} s_*^{1/28} R_{r,5}^{1/14} R_{c,4}^{-1/2} \zeta_6^{1/12} Q^{-1/7} \text{ K}, \quad (22)$$

respectively.

In Table 2, we compare between the observed (second-fourth columns) and predicted (fifth-eighth columns) X-ray and  $\gamma$ -ray emission properties. For the effective radii of the rim and core components, (1) we apply the observational value if it is available or (2) we apply the typical value  $R_r = 3 \times 10^5 \text{ cm}$  and  $R_c = 10^4 \text{ cm}$ , respectively, if observational results are unavailable. In addition, we use the curvature radii corresponding to  $s_* = 0.5$  and  $\zeta_6 = 1$ . We find in Table 2 that the predicted surface temperatures of the rim ( $T_r^p \sim 0.5 - 0.7 \times 10^6 \text{ K}$ ) and core components ( $T_c^p \sim 1 - 4 \times 10^6 \text{ K}$ ) are approximately consistent with the observations. The predicted  $\gamma$ -ray luminosity  $L_\gamma^p \sim 5 \times 10^{32} \text{ erg s}^{-1}$  is consistent with the observations for older MSPs with  $\tau_c > 5 \times 10^9 \text{ yrs}$ , where  $\tau_c \equiv \dot{P}/(2P) \sim 1.5 \times 10^9 P_{-3}^2 / \mu_{26}^2 \text{ yrs}$  (Table 1). For the younger MSPs (PSRs J0218+4232, B1937+21 and B1957+20), we find that the outer gap model predicts a  $\gamma$ -ray luminosity one order of magnitude less than that from the *Fermi* observation.

### 3.2. Outer gap controlled by the magnetic pair-creation process

Takata et al. (2010b) argued that the incoming particles emit photons with an energy  $m_e c^2 / \alpha_f \sim 70 \text{ MeV}$  by curvature radiation near the stellar surface. These photons can become pairs via the magnetic pair creation process and the secondary pairs can continue to radiate several MeV photons via synchrotron radiation. In this case, the photon multiplicity can easily exceed  $10^4$  per incoming particle. For a simple dipole field structure, all pairs move inward and cannot affect the outer gap accelerator. However if the local field lines near the surface are bent sideward due to the strong multipole field (e.g. shown in Figure 2), the pairs created in these local magnetic field lines can have an angle greater than  $90^\circ$ , which results in an outgoing flow of pairs. Only a very tiny fraction (1-10) out of  $10^4$  photons is required to create pairs in these field lines, which are sufficient to provide screening in the outer gap when they migrate to the outer magnetosphere. In this model, the fractional gap thickness in this circumstance is

$$f_m \sim 0.025 K P_{-3}^{1/2}, \quad (23)$$

where  $K \sim B_{m,12}^{-2} s_7$  characterizes the local parameters. Here,  $B_{m,12}$  and  $s_7$  are the local magnetic field in units of  $10^{12} \text{ G}$  and the local curvature radius in units of  $10^7 \text{ cm}$ , respectively. For the case of MSPs, the local parameter can be in the range  $B_{m,12} \sim 0.01 - 0.1$  and  $s_7 \sim 0.01 - 0.1$ , which yields  $K$  of the order of ten. Substituting equation (23) into equations (5) and (4), we obtain the expected  $\gamma$ -ray luminosity and the typical radiation energy as

$$L_\gamma^m \sim 6 \times 10^{33} K_1^3 P_{-3}^{-5/2} \mu_{26}^2 \text{ erg s}^{-1}, \quad (24)$$

and

$$E_c^m \sim 3 K_1^{3/2} P_{-3}^{-1} \mu_{26}^{3/4} s_*^{-1/4} \text{ GeV}, \quad (25)$$

respectively, where  $K_1 = K/10$ . The total X-ray luminosity and the temperatures of the heated surface are described as

$$L_X^m \sim 3 \times 10^{31} K_1 P_{-3}^{-7/6} \mu_{26} \text{ erg s}^{-1}, \quad (26)$$

$$T_r^m \sim 10^6 K_1^{1/4} P_{-3}^{-7/24} \mu_{26}^{1/4} R_{r,5}^{-1/2} Q^{1/4} \text{ K}, \quad (27)$$

and

$$T_c^m \sim 4 \times 10^6 K_1^{1/4} P_{-3}^{-3/8} \mu_{26}^{1/4} R_{c,4}^{-1/2} \zeta_6^{1/12} \text{ K}, \quad (28)$$

respectively.

The X-ray and  $\gamma$ -ray emission properties predicted by the outer gap model controlled by the magnetic pair-creation process near the stellar surface are summarized in ninth-twelfth columns of Table 2. By comparing between the emission properties predicted by

the photon-photon pair-creation model and the magnetic pair-creation model in Table 2, we find that the X-ray/ $\gamma$ -ray emission properties for the older MSPs do not depend strongly on the specific pair-creation process controlling the outer gap. For younger MSPs (PSRs J0218+4232, B1937+21 and B1957+20), however, the magnetic pair-creation model predicts  $\gamma$ -ray emission about one order of magnitude brighter than that of the photon-photon pair-creation model in closer agreement with the *Fermi* observation.

For PSR J1614-223 (or J0437-4718), the theoretical predictions in Tables 2 are found to lie below (exceed) the measured value. This discrepancy may be affected by the local structure, since the  $\gamma$ -ray luminosity described by equation (24) is sensitive to the local structure as  $L_\gamma \propto K^3$ . Furthermore the uncertainties of the solid angle and the distance may also contribute to these discrepancies. As indicated in Table 1, the observed flux of PSR J1614-223 implies a  $\gamma$ -ray emission efficiency of  $L_\gamma/L_{sd} \sim 1$  assuming a solid angle  $\Delta\Omega_\gamma = 4\pi$  and distance  $d = 1.3$  kpc. Comparing with the expected efficiency  $L_\gamma/L_{sd} \sim 0.1$  for the outer gap model, the actual solid angle and/or distance may be several factors smaller than  $\Delta\Omega_\gamma = 4\pi$  and/or  $d = 1.3$  kpc. In addition to the local effect and the observational parameters, the observed inefficient  $\gamma$ -ray luminosity of PSR J0437-4718 may be a result of an unfavorable viewing angle. Takata et al. (2001a,b,c) showed that the observed  $\gamma$ -ray flux from the outer gap decreases with decreasing viewing angle as measured from the spin axis. Hence, *Fermi* has preferentially discovered pulsars with larger viewing angle  $\xi \sim 90^\circ$ . For the  $\gamma$ -ray pulsars with  $\xi \sim 90^\circ$ , the luminosity inferred from the flux can be characterized by equation (24). On the other hand, if the viewing angle is much smaller than  $90^\circ$ , the  $\gamma$ -ray luminosity inferred from the observed flux will lie below the prediction (24). In fact, a smaller Earth viewing geometry is preferred to reproduce the observed single pulse profile of PSR J0437-4718 (Abdo et al. 2009b) using the outer gap model (Takata et al. 2011c).

Based on statistical grounds, Takata et al. (2010b) suggest that the outer gap controlled by the pair-creation model may provide a preferable explanation for the possible observational correlation between the characteristics of the  $\gamma$ -ray emission and the pulsar characteristics. For the MSPs, the  $\gamma$ -ray luminosity  $L_\gamma$  (18) and (24) can be cast in terms of the spin down power  $L_{sd} = 2(2\pi)^4\mu/(3c^3P^4)$  or the characteristic age  $\tau_c = P/2\dot{P}$  yielding

$$L_\gamma^p \sim 3 \times 10^{32} L_{sd,34}^{1/14} \mu_{26}^{1/7} s_*^{1/7} R_{r,5}^{2/7} Q^{-1/7} \text{ erg s}^{-1}, \quad (29)$$

or

$$L_\gamma^p \sim 4 \times 10^{32} \tau_{c,9}^{-1/7} s_*^{1/7} R_{r,5}^{2/7} Q^{-1/7} \text{ erg s}^{-1} \text{ erg s}^{-1}, \quad (30)$$

for the outer gap controlled by the photon-photon pair-creation process, and

$$L_\gamma^m \sim 6 \times 10^{32} L_{sd,34}^{5/8} K_1^3 \mu_{26}^{3/4} \text{ erg s}^{-1}, \quad (31)$$

or

$$L_\gamma^m \sim 10^{34} \tau_{c,9}^{-5/4} K_1^3 \mu_{26}^{-1/2} \text{ erg s}^{-1}, \quad (32)$$

by the magnetic pair-creation process. Here,  $L_{sd,34} = (L_{sd}/10^{34} \text{ erg s}^{-1})$  and  $\tau_{c,9} = (\tau_c/10^9 \text{ yrs})$ . In Figures 3 and 4, the model predictions given by equations (29)-(32) are plotted with the solid lines (for the photon-photon pair-creation) or dashed lines (for the magnetic pair-creation). The filled circles represent the MSPs detected by the *Fermi*-LAT. Notwithstanding the large observational errors, the data points at large  $L_\gamma$  in Figures 3 and 4 may suggest that the magnetic pair-creation model is preferred over the photon-photon pair-creation model for the  $L_\gamma - L_{sd}$  and  $L_\gamma - \tau_c$  relations.

Given that the X-rays from the heated polar cap may be prevented from illuminating the outer gap by the resonant cyclotron scattering process, the magnetic pair-creation process may be the more important process to control the outer gap. The cross section for Thomson scattering can be represented as (Halpern & Ruderman 1993; Zhang & Cheng 1997),

$$\sigma = \sigma_T (\hat{\varepsilon} \cdot \hat{B})^2 + \frac{2\pi^2 e^2}{m_e c} (\hat{\varepsilon} \times \hat{B})^2 \delta(\omega_B - \omega), \quad (33)$$

where  $\hat{\varepsilon}$  is the (electric field) polarization of the X-ray photons,  $\hat{B}$  is the unit vector of the direction of the background magnetic field and  $\omega_B = eB(r)/mc$ . In the case where  $\hat{\varepsilon} \cdot \hat{B} = 0$  and for a local dipole magnetic field  $B_s \sim 10^{11} \text{ G}$ , the resonant scattering will be efficient at  $\delta R \sim l(B_s e \hbar / E_X m_e c)^{1/3} \sim 7 \times 10^5 \text{ cm} (l/3 \cdot 10^5 \text{ cm}) (B_s/3 \times 10^{11} \text{ G})^{1/3} (T/10^6 \text{ K})^{-1/3}$  from the stellar surface, where  $l$  is the thickness of the crust. Since we obtain

$$\int \sigma dr \sim \frac{2\pi^2 e^2}{m_e c \omega} \left( \frac{e B_s l^3}{m_e c \omega} \right)^{1/3} \sim 10^{-13} \left( \frac{l}{3 \cdot 10^5 \text{ cm}} \right) \left( \frac{B_s}{3 \cdot 10^{11} \text{ G}} \right)^{1/3} \left( \frac{T}{10^6 \text{ K}} \right)^{4/3} \text{ cm}^3, \quad (34)$$

a number density  $n_\pm > 10^{13} \text{ cm}^{-3}$  at  $\delta R \sim 10^6 \text{ cm}$  leads to an optically thick cyclotron resonant scattering layer. The number density of the incoming primary particles near the stellar surface, which may be about 50 % of the Goldreich-Julian value (e.g. equation 12), becomes  $n \sim B/(2Pce) \sim 3 \times 10^9 (B/10^8 \text{ G}) P_{-3}^{-1} \text{ cm}^3$ . This value implies that the cyclotron resonant scattering can become optically thick for the multiplicity of the incoming particles due to the magnetic pair-creation ( $\geq 10^4$ , see Takata et al. 2010b). Because the radial distance to the inner boundary of the outer gap from the stellar surface is only  $\sim 5 \times 10^6 - 10^7 \text{ cm}$  for MSPs, it is possible that the scattering layer prevents the illumination of the inner part of the outer gap by X-ray photons. In such a case, the magnetic pair-creation process can control the outer gap.

## 4. Application to Millisecond Pulsar in Quiescent LMXBs

### 4.1. Thermal X-ray emissions from MSPs

Observations of the optical modulation of LMXBs in the quiescent state have provided indirect evidence for additional heating of the companion star, possibly due to the rotational energy loss of the NS associated with pulsar activity, e.g. J102347.68+003841.2 (Thorstensen & Armstrong 2005), SAX J1808.4-3658 (Burderi et al. 2003; Deloye et al. 2008), XTE 1814-338 (D’Avanzo et al. 2009) and IGR J00291+5934 (Jonker, Torres & Steeghs 2008). Specifically, the irradiation luminosity required to produce the amplitude of the modulation is  $\sim 10^{33-34}$  erg s $^{-1}$  for the isotropic radiation. This is significantly greater than that associated with the X-ray emission from the disk or neutron star, indicating the need for the operation of an additional heating source. If the pulsar magnetosphere is sufficiently clear of matter during the quiescent state of the LMXB, the outer gap accelerator can be activated and the emitted  $\gamma$ -rays may irradiate and heat the companion star. If the optical modulation is a result of irradiation from the outer gap, the actual irradiated luminosity may be several factors less than that for the isotropic case because the outer gap emission is beamed with a solid angle  $\Delta\Omega_\gamma \sim 2 - 3$  radian (Takata et al. 2010b). The amplitude of the optical modulation is estimated as  $L_o \sim (\pi\theta^2/\Delta\Omega_\gamma)L_\gamma$ , where  $\theta$  is the angle of the size of the companion star measured from the pulsar and  $\Delta\Omega_\gamma$  is the solid angle of the  $\gamma$ -ray beam. If the companion fills its Roche lobe,  $\theta \sim 0.462[q/(1+q)]^{1/3}$  for typical LMXB  $0.1 < q < 0.8$ , where  $q$  is the mass ratio of the system (Frank, King & Raine, 2002).

Deep X-ray observations have been carried out during the quiescent state to search for the thermal emission from the NS star surface. The detected emissions indicate that the NS is hotter in comparison to expectations based on traditional cooling curves of NSs. An explanation for this difference is a consequence of heating associated with nuclear fusion in the crust. In this picture, the base of the accreted matter in the crust is sufficiently compressed by the overlying weight of newly accreted matter, leading to pycnonuclear reactions at  $\rho \sim 10^{12-13}$  g cm $^{-3}$ . These reactions release about 1-2 MeV per accreted baryon, resulting in heating of the crust and the core (Brown, Lars & Rutledge 1998; Haensel & Zdunik 1990, 2003). On a time scale of  $10^4$  yr, thermal equilibrium is established between heating during the accretion stage and cooling during the quiescent stage (Colpi et al. 2001). Accordingly, the NS core and surface temperatures can reach  $\sim 10^{8-9}$  K in the interior and  $\sim 10^6$  K at the surface. Given this surface thermal emission, the outer gap in the quiescent stage may be controlled by the photon-photon pair-creation between the  $\gamma$ -rays and the X-rays from the NS surface.

To explore the  $\gamma$ -ray emission from AMPs in the quiescent state, the X-ray emission in



this state is calculated following the model description by Yakovlev et al. (2003). The NS core temperature,  $T_i$ , surface temperature,  $T_s$ , and long-term time-average ( $\sim 10^4$  yr) mass accretion rate,  $\langle \dot{M} \rangle$ , are related by

$$L_h(\langle \dot{M} \rangle) = L_\nu(T_i) + L_{th}(T_s), \quad (35)$$

where  $L_h$  is heating term due to the pycnonuclear reactions,  $L_\nu$  is cooling term associated with neutrino emission, and  $L_{th} = 4\pi R_s^2 \sigma_s c T_s^4$  is the thermal emission from the NS surface. The heating rate is expressed as

$$L_h(\langle \dot{M} \rangle) = \frac{\langle \dot{M} \rangle}{m_u} Q_\nu \sim 8.7 \times 10^{33} \frac{\langle \dot{M} \rangle}{10^{-10} \text{ M}_\odot \text{ yr}^{-1}} \text{ erg s}^{-1}, \quad (36)$$

where  $m_u$  is the atomic mass unit and  $Q_\nu \sim 1.45$  MeV is the nuclear energy release per baryon. The neutrino emission  $L_\nu$  is calculated using equation (4) in Yakovlev et al. (2003). A  $T_i - T_s$  relation was obtained by Gudmundsson, Pethick, & Epstein (1983) as

$$T_i \sim 1.288 \times 10^8 (T_{s,6}^4 / g_{14})^{0.455} \text{ K}, \quad (37)$$

where  $g_{14}$  is the surface gravity  $g = GM e^{-\Phi} / R^2$  in units of  $10^{14} \text{ cm s}^{-2}$ . Here,  $\Phi = \sqrt{1 - 2GM/c^2 R_s^2}$  and  $T_{s,6} = T_s / 10^6 \text{ K}$ .

Figures 5 and 6 display the X-ray luminosity and the surface temperature in the quiescent state as a function of the averaged accretion rate respectively. The different lines correspond to cooling of a low mass NS (solid line) and various enhanced cooling mechanisms for high mass NSs. In Figures 5 and 6, the observational data for various quiescent LMXBs are given for reference, based on the work by Heinke et al. (2009).

## 4.2. $\gamma$ -ray emissions from the outer gap

### 4.2.1. $\gamma$ -ray luminosity

Using the pair-creation condition  $E_\gamma E_X = (m_e c^2)$  with  $E_X = 3kT$ , the relation between the fractional gap thickness and the surface temperature is given as

$$f \sim 0.12 P_{-3}^{7/6} \mu_{26}^{-1/2} s_*^{1/6} T_{s,6}^{-2/3}, \quad (38)$$

yielding a  $\gamma$ -ray luminosity in the quiescent state corresponding to

$$L_\gamma \sim 6 \times 10^{32} P_{-3}^{-1/2} \mu_{-26}^{1/2} s_*^{1/2} T_{s,6}^{-2} \text{ erg s}^{-1}. \quad (39)$$

Figure 7 represents the predicted  $\gamma$ -ray luminosity for four LMXBs (SAX J1808.4-3658, XTE J0929-314, XTE J1814-328 and IGR J00291-5934) as a function of the averaged accretion rate. The solid line (for the low mass NS) and dashed line (for the high-mass NS with nucleon matter) represent the results for the outer gap model controlled by the photon-photon pair-creation process between the  $\gamma$ -rays and the X-ray from the full surface cooling emissions. Furthermore, the dotted and dotted-dashed horizontal lines represent results for the outer gap model controlled by the photon-photon pair-creation process between the  $\gamma$ -ray and the X-rays from the heated polar cap region and by the magnetic pair-creation process near the stellar surface respectively. Since the magnetic fields for the MSPs in quiescent LMXBs have not been constrained, we present the results for two extreme cases as thick and thin lines. For the thick lines, we assume that  $\mu_{26} = 1.5P_{-3}^{7/6}$ , which gives an upper limit of the magnetic field for the recently turned on the radio millisecond pulsar PSR J1023+0038 (see Figure 1). For the thin-lines, on the other hand, we estimate the dipole magnetic field from  $\mu_{26} = P_{-3}^{7/6}/3$ , which describes the relation for the MSPs detected by *Fermi*-LAT.

It can be seen in Figure 7 that the predicted  $\gamma$ -ray luminosity given by the solid and dashed lines increases with decreasing time averaged accretion rates. This dependence reflects the fact that the surface temperature decreases with a decrease of the averaged accretion rate, as Figure 6 reveals. In the present case, the fractional gap thickness is related with the surface temperature as  $f \propto T_{s,6}^{-2/3}$ , indicating that the gap is thicker for lower accretion rates. Since the  $\gamma$ -ray luminosity is expressed by  $L_\gamma \sim f^3 L_{sd}$ , the predicted  $\gamma$ -ray luminosity increases with a decrease of the averaged accretion rate. We note that the predicted  $\gamma$ -ray luminosity presented in Figure 7 is insensitive to the spin periods of the known MSPs in the quiescent LMXBs because it is assumed that  $\mu \propto P^{7/6}$ , which results in  $L_\gamma \propto P^{1/12}$ .

#### 4.2.2. Irradiation of $\gamma$ -rays to companion star

To explain the observed optical modulation of the companion star in quiescent state, Takata et al. (2010a) discussed the irradiation of  $\gamma$ -rays from the outer gap to the companion star. The magnetospheric  $\gamma$ -ray irradiating the companion star may be absorbed via the so-called pair-creation process in the Coulomb field by the nuclei in the stellar matter. Further absorption will occur as the relativistic pairs created with a Lorentz factor  $\Gamma \sim 10^3$  will transfer their energy and momentum to the stellar matter via the ionization and/or the Coulomb scattering processes. The cross section of the above pair-creation process for the photon with energy  $E_\gamma$  is given by Lang (1999) as

$$\sigma(E_\gamma) = 3.5 \times 10^{-3} Z^2 \sigma_T \left[ \frac{7}{9} \log \left( \frac{183}{Z^{1/2}} \right) - \frac{1}{53} \right] \quad \text{for } \frac{E_\gamma}{2} \gg \frac{m_e c^2}{\alpha Z^{1/3}}, \quad (40)$$

where  $Z$  is the atomic number,  $\sigma_T$  is the Thomson cross section. All  $\gamma$ -rays irradiating the star can be absorbed if the column density of the star exceeds

$$\Sigma > \frac{m_p}{\sigma} \sim 60 \text{ g cm}^{-2}, \quad (41)$$

where we use  $Z^2 = 3$  appropriate for the solar abundance. We can see that the above condition is easily satisfied for the typical low mass companion star, which has  $\sim 0.1 M_\odot$  and the radius  $\sim 10^{10}$  cm.

The created pairs will transfer their energy to the stellar matter via exciting and ionizing atoms in the matter. For atomic hydrogen, the energy loss rate of the pairs per unit length is given by Lang (1999) as

$$\frac{dE}{dx} \sim -2.54 \times 10^{-19} N_e W \text{ eV cm}^{-1} \quad (42)$$

where  $N_e$  is the number density of the electrons in the matter, and  $W$  is a factor of 10-100. All energy of the created pairs will transfer to the stellar material if the column density of the star exceeds

$$\Sigma > 70 \left( \frac{E}{1\text{GeV}} \right) \left( \frac{W}{100} \right)^{-1} \text{ g cm}^{-2}, \quad (43)$$

which is easily satisfied for the typical companion star. Hence, all of the irradiation energy from the outer gap will transfer to the stellar matter.

In Figure 7, the observational data represents the lower limit of the irradiating luminosity  $L_{irr}$  required to explain the optical modulation. We find that if the optical modulation originates from the irradiation of the  $\gamma$ -rays from the outer gap of the pulsar magnetosphere, the observations can constrain the theoretical model. For example, the level of the inferred irradiation luminosity  $L_{irr} \sim 10^{34} \text{ erg s}^{-1}$  of SAX J1808.4-3658, XTE J1814-325 and IGR J00291+5934 suggests that the outer gap with the high-mass NS model is preferable. The outer gap model with low mass NS predicts, on the other hand, a lower  $\gamma$ -ray luminosity by an order of magnitude due to the higher NS surface temperatures and may be applicable to J0929-314.

It should be noted that  $L_{irr} \sim 10^{34} \text{ erg s}^{-1}$  cannot be produced by the outer gap model controlled by the photon-photon pair-creation process between the  $\gamma$ -rays and the X-rays from the heated polar cap region. Within the context of the present treatment for the magnetic field determination, that is  $\mu_{26} = \kappa P_{-3}^{7/6}$ , where  $\kappa$  is the proportional factor, the  $\gamma$ -ray luminosity described by equation (18) is less dependent on the proportional factor  $\kappa$ . That is,  $L_\gamma \propto \kappa^{2/7}$  and unrealistic values, say  $\kappa \sim 1000$  are required to produce  $L_\gamma \sim 10^{34} \text{ erg s}^{-1}$ . However, such a model would not be consistent with the properties

of the quiescent X-ray emission. On the other hand,  $L_\gamma \propto \kappa^2$  for the outer gap with the magnetic pair-creation process implies that such a model can produce  $L_\gamma \sim 10^{34} \text{ erg s}^{-1}$  with a reasonable value of the NS magnetic field. As indicated by the dashed-dotted lines in Figure 7 (also Figure 9), the model prediction is sensitive to the specific relation between the spin period and magnetic moment. Hence a measurement the possible  $P - \mu$  relation for the accreting MSPs is desired for further discussion on the origin of  $\gamma$ -ray emission from the MSPs in quiescent LMXBs.

## 5. Magnetospheric Non-thermal X-ray emissions from MSPs

### 5.1. Rotation powered MSPs

The  $\gamma$ -rays ( $> \text{GeV}$ ) from the outer gap may be converted into pairs via the photon-photon pair-creation process involving the thermal X-rays from the NS surface before escaping the magnetosphere. The secondary pairs produced near the light cylinder, where the magnetic field  $B \sim 10^{5-6} \text{ G}$ , will emit non-thermal X-rays via the synchrotron radiation process with a typical energy of  $E_{n,X} \sim 2(\Gamma/10^3)^2 (B/10^6 \text{ G})^2 (\sin \theta/0.1) \text{ keV}$ . Here,  $\Gamma_s \sim (1 \text{ GeV}/2m_e c^2)$  is the typical Lorentz factor of the secondary pairs, and  $\theta$  is the pitch angle. The synchrotron damping length of the secondary pairs is  $l_d \sim 1.5 \times 10^6 (\Gamma_s/10^3)^{-1} (B \sin \theta/10^5)^{-2} \text{ cm}$ , implying the secondary pairs quickly lose their perpendicular momentum inside the light cylinder. In such a case, the luminosity of the non-thermal X-rays is estimated as

$$L_{n,X} \sim \tau_{X\gamma} L_\gamma, \quad (44)$$

where  $\tau_{X\gamma} (< 1)$  is the optical depth of the photon-photon pair-creation process. Note that because the local cyclotron energy near the light cylinder is less than the X-ray energy, the resonant scattering is inefficient near the light cylinder, implying the non-thermal X-rays can freely escape from the magnetosphere.

It can be seen from equations (13)-(16) that the ratio of the photon number density, which is proportional to  $L_r/T_r$ , of the rim component is about a factor of ten larger than that of the core component, indicating the optical depth  $\tau_{X\gamma}$  near the light cylinder can be estimated as

$$\tau_{X\gamma} \sim \frac{L_r}{4\pi R_{lc}^2 c E_r} \sigma_{X\gamma} R_{lc} \sim 0.014 f^{3/4} P_{-3}^{-9/4} \mu_{26}^{3/4} R_{r,5}^{1/2} Q^{3/4}. \quad (45)$$

Here,  $E_r = 3kT_r$  and  $\sigma_{X\gamma} \sim \sigma_T/3$  with  $\sigma_T$  corresponding to the Thomson cross section. Inserting the gap fractions described by equations (17) and (23) into equation (44), the non-thermal X-ray luminosity can be expressed as a function of the spin-down power as

$$L_{n,X} \sim 5 \times 10^{29} L_{sd,35}^{45/112} \mu_{26}^{-11/56} s_*^{15/28} R_{r,5}^{11/7} Q^{3/14} \text{ erg s}^{-1} \quad (46)$$

for the outer gap model controlled by the photon-photon pair-creation process and

$$L_{n,X} \sim 6 \times 10^{30} L_{sd,35}^{35/32} K_1^{15/4} \mu_{26}^{3/8} R_{r,5}^{1/2} Q^{3/4} \text{ erg s}^{-1}, \quad (47)$$

by the magnetic pair-creation process. The model results described by equations (46) and (47) are plotted in Figure 8 with the solid and dashed lines respectively. For the observational data in Zavlin (2007), we represent the *Fermi* MSPs with the filled circles and the radio MSPs with filled triangles. We find in Figure 8 that the outer gap model controlled by the magnetic pair-creation process can explain the observed possible correlation between the non-thermal X-ray luminosity and the spin down power slightly better than the model controlled by the photon-photon pair creation process.

For the synchrotron emission from the secondary pairs, it is expected that the spectrum is described by a photon index of  $\alpha \sim 1.5$  below  $E < E_{n,X}$  (Takata, Chang & Cheng 2007). On the other hand, the secondary particles will escape from the light cylinder with a Lorentz factor  $\Gamma_c \sim 5 \times 10^2$ , for which the synchrotron damping length is comparable to the light cylinder radius. We expect that the emission of the secondary pairs beyond the light cylinder is not observed as pulsed emission because the co-rotation motion with central star can not be retained beyond the light cylinder. In such a case, the observed pulsed emissions has a break at the energy of  $E_c \sim 400 (\Gamma_c/5 \cdot 10^2)^2 (B/10^6)(\sin \alpha/0.1) \text{ eV}$ , below which the spectrum is characterized by a photon index  $\alpha = 2/3$ , which corresponds to the spectrum described by the emission from the single particle. Hence, the present model predicts that the non-pulsed X-ray emissions from rotation powered MSPs are described by spectra with a photon index  $\alpha = 2/3 - 1.5$ , which may not be in conflict with the observed range  $\alpha \sim 1 - 2$  (Zavlin 2007). Furthermore, the present model predicts that a spectral cut-off of the secondary emissions appears at  $E_{n,X} \sim 2(\Gamma/10^3)^2 (B/10^6 \text{ G})^2 (\sin \theta/0.1) \text{ keV}$ . If the cut-off energy position is located in the observation energy range, the photon index fit to the observed spectrum with the single power law function can be larger than  $\alpha = 1.5$ .

## 5.2. Accretion powered pulsars in quiescent LMXBs

The predicted relation between the non-thermal X-ray luminosity in the quiescent state and the averaged accretion rate for LMXBs is summarized in Figure 9. The non-thermal X-ray luminosity is calculated from  $L_{n,X} \sim \tau_{X\gamma} L_\gamma$ , where the optical depth  $\tau_{X\gamma}$  is given by  $\tau_{X\gamma} = L_{th}(T_s) \sigma_{X\gamma} / (4\pi R_{lc} c E_s)$  with  $E_s = 3kT_s$ . The thermal X-ray luminosity  $L_{th}$  and the surface temperature  $T_s$  correspond to the results represented in Figures 5 and 6, respectively. In addition, we calculate the expected  $\gamma$ -ray luminosity  $L_\gamma$  with  $P = 2.5 \text{ ms}$  of SAX J1808.4-3658 for reference. Note that the calculated X-ray luminosity is not sensitive to the spin

periods in the observed range of presently known MSPs in quiescent LMXBs. In Figure 9, the solid and dashed lines represent the non-thermal X-ray luminosity for the low-mass NS and the high mass NS models with nucleon matter cooling processes respectively. The thick and thin lines represent the results for magnetic fields determined from  $\mu_{26} = 1.5P_{-3}^{7/6}$  and  $\mu_{26} = P_{-3}^{7/6}/3$  respectively. For comparison, we plot the model predictions if the outer gap is controlled by the photon-photon pair-creation with the X-rays from the heated polar cap (dotted lines) and by the magnetic pair-creation process near the NS surface (dashed-dotted lines) respectively.

For the case of the outer gap controlled by the surface X-ray emission (solid and dashed lines) in Figure 9, we find that the predicted non-thermal X-ray luminosity decreases with decreasing time averaged mass accretion rates, although the  $\gamma$ -ray luminosity increases as Figure 7 shows. This results from the fact that the number of the thermal X-ray photons, which absorb the  $\gamma$ -ray photons in the outer magnetosphere, decreases with a decrease of the accretion rate, and the decrease of the thermal X-ray luminosity is more rapid than the increase of the  $\gamma$ -ray luminosity, as Figures 7 and 9 show. As a result, the present non-thermal X-ray luminosity, which is proportional to  $L_{n,X} \sim \tau_{X\gamma} L_{\gamma} \propto L_{th}(< \dot{M} >) L_{\gamma}$ , decreases with the decrease of the accretion rate. It is also found in Figure 9 that the non-thermal X-ray luminosity is less dependent on the accretion rate in comparison with the  $\gamma$ -ray luminosity. For example, if the accretion rate changes between  $10^{-13} \text{ M}_{\odot} \text{ yr}^{-1}$  and  $10^{-8} \text{ M}_{\odot} \text{ yr}^{-1}$ , the X-ray luminosity varies less than factor of ten (see Figure 9), whereas the  $\gamma$ -ray luminosity varies more than factor of ten (see Figure 7).

Finally, it has been known that X-ray emission (0.5-10 keV) from SAX J1808.4-3658 in quiescence is well fit by a power law spectrum with a photon index of  $\alpha \sim 1.4 - 2$  and with a luminosity of  $L_{n,X} \sim 10^{31-32} \text{ erg s}^{-1}$  (Heinke et al. 2009). Because the pulsed period in the non-thermal X-ray emissions has not been confirmed yet, its origin is still unclear. As Figure 9 indicates, if the non-thermal X-ray emission originates from the magnetosphere, the outer gap model with the low-mass X-ray NS or with the magnetic pair-creation process for the gap closing may be more favorable, although the observational error is large. As we discussed in section 4.2.2 (c.f. Figure 7), the optical modulation of the companion star observed during the quiescent state can be explained by  $\gamma$ -ray irradiation from the outer gap with the high-mass X-ray NS or with the magnetic pair-creation process for the gap closing. For the high-mass NS model, the predicted non-thermal X-ray luminosity associated with the outer gap may be insufficient to explain the observational result, as Figure 9 shows, indicating the need for an additional component. In this case, the non-thermal emission originating from the interaction between the pulsar wind and the stellar wind via an intra-binary shock may be observable, as we will discuss in section 6.

## 6. High-energy emissions from intra-binary shock

Stappers et al. (2003) detected the unresolved X-ray emission around a binary system composed of the millisecond pulsar (PSR B1957+20) and low mass star (LMS), in which the wind of the companion star eclipses the pulsed radio emission for  $\sim 10\%$  of every orbit. They suggested that the pulsar wind is ablating the low-mass companion star, and that the observed unpulsed X-ray emission from the PSR B1957+20 binary system originates from the interaction between the pulsar wind and the stellar wind via an intra-binary shock (Arons & Tavani 1993; Cheng, Taam & Wang 2006). Similar binary systems, so called “black widow” systems, in which the MSP is destroying a low mass companion star, has also been discovered as *Fermi*  $\gamma$ -ray sources in the Galactic field (Table 3), suggesting the existence of high energy particles in the “black widow” system (Roberts et al. 2011). For AMP, the intra-binary shock in quiescent state is also suggested to explain the observed non-thermal X-ray emission from SAX J1808.4-3658 (e.g. Campana et al. 1998).

The high-energy emission from an intra-binary shock between a pulsar and a high-mass companion star has been established for so called  $\gamma$ -ray binary PSR B1256/LS 2883 system, which is composed of a canonical radio pulsar with a period of  $P \sim 48$  ms and high mass Be star (Tam et al. 2011; Abdo et al. 2011; Aharonian et al. 2009). In the  $\gamma$ -ray binary, it has been proposed that the shock stands at the interface between the pulsar wind and the Be wind/disk, and unpulsed radio to TeV radiations are produced via the synchrotron and inverse Compton processes of the accelerated particles at the shock (Tavani & Arons 1997; Takata & Taam 2009; Kong et al. 2011). The observed photon index in the X-ray bands from the  $\gamma$ -ray binary varies with the orbital phase in the range  $\alpha = 1 - 2$ .

For a pulsar/low mass star binary, Arons & Tavani (1993) proposed the intra-binary shock model to explain the unpulsed X-ray emissions from the PSR B1957+20/LMS system (see also Cheng et al. 2006). In particular, the separation between the pulsar and the companion star is order of  $a_o \sim 10^{10-11}$  cm, which is about 2-3 orders of magnitude smaller than  $a_o \sim 1$  AU of pulsar/high mass star system, PSR B1256/LS 2883. Therefore, if the observed non-thermal X-ray emission from PSR B1957+20, is produced by an intra-binary shock, the MSP/LMS system (i.e., black widow system) provides a unique laboratory to probe the physics of the pulsar wind in the vicinity of the neutron star. In this section, therefore, we discuss the emission from the intra-binary shock in pulsar/LMS systems, and examine the predicted  $\gamma$ -ray and X-ray luminosity for known black widow systems.

It has been pointed out that the synchrotron emission from the shock caused by the interaction between the pulsar wind and ISM contributes to the resolved X-ray nebula around PSR 1957+20 (Stappers et al. 2003; Huang & Becker 2007; Cheng et al. 2006). On the other hand, we expect that the emission from the pulsar wind nebula does not extend to  $\gamma$ -ray



bands, and therefore is not a candidate for the origin of the  $\gamma$ -ray emission detected by the *Fermi* observations. The Lorentz factor of the accelerated particles at the shock between pulsar wind and ISM may be limited below the critical value, at which the gyroradius,  $r_g = \Gamma m_e c^2 / eB$ , is equal to the size of the shock. Assuming the shock size  $r_s \sim 5 \times 10^{16}$  cm and the magnetic field  $B \sim 10^{-5}$  G (Cheng et al. 2006), the Lorentz factor is limited below  $\Gamma = 3 \times 10^8 (B/10^{-5} \text{G})(r_s/5 \cdot 10^{16} \text{cm})$ . This indicates that the synchrotron spectrum extends up to the hard X-ray bands,  $E_c \sim (3h\Gamma^2 eB/4\pi m_e c) \sim 15(B/10^{-5} \text{G})^3 (r_s/5 \cdot 10^{16} \text{cm})^2 \text{keV}$ , implying the spectrum can not extend in  $\gamma$ -ray energy bands. We, henceforth, examine the high-energy emission from an intra-binary shock and from the magnetosphere in black widow systems as possible sites for the origin of the  $\gamma$ -ray emissions indicated by the *Fermi* observations.

The distance ( $r_s$ ) from the pulsar to the intra-binary shock may be estimated by the pressure balance as

$$\frac{L_{sd}}{4\pi r_s^2 c} = \frac{\dot{M} v_g}{4\pi f_w (a_o - r_s)^2}, \quad (48)$$

where we assumed that the pulsar wind is emitted with the solid angle  $4\pi$ ,  $\dot{M}$  is the mass loss rate from the star,  $v_g$  is the velocity for gaseous material, and  $f_w$  is the outflow fraction in units of  $4\pi$ . For the black widow system, PSR B1957+20, the mass loss rate from LMS is expected as  $\dot{M}_c \sim M_c \dot{P}_b P_b^{-1} \sim 10^{-10} M_\odot \text{ yr}^{-1}$ , where  $M_c = 0.02 M_\odot$  is the mass of LMS,  $P_b = 33001$  s is the orbital period and  $\dot{P}_b \sim 10^{-11}$  is the orbital period derivative (Fruchter et al. 1990). For the quiescent LMXBs, the mass loss rate will be smaller than  $\dot{M} \sim 10^{-11} - 10^{-12} M_\odot \text{ yr}^{-1}$ , based on the study by Heinke et al. (2009).

With the mass-loss rate of  $\dot{M} \sim 10^{-10} - 10^{-12} M_\odot \text{ yr}^{-1}$ , we find that the shock distance from the pulsar is of the order of the orbital separation. For example, if we assume the stellar wind velocity is the escape velocity from the system, we obtain  $v_g \sim \sqrt{2GM_\odot/a_o} \sim 10^8 \text{ cm s}^{-1}$ , where  $a_o \sim 5 \times 10^{10}$  cm is the typical separation between two components. Using  $L_{sd} = 10^{34} \text{ erg s}^{-1}$ ,  $\dot{M} = 10^{-11} M_\odot \text{ yr}^{-1}$ ,  $a_o = 5 \times 10^{10}$  cm, and  $f_w = 1$ , the equation (48) implies the shock distance of  $r_s \sim 3.5 \times 10^{10}$  cm. Hence, the shock radius from the pulsar will be of order of the separation between two components.

We assume that the kinetic energy dominated flow of the pulsar wind is formed within the distance  $r \sim a_o$  from the pulsar, that is, the so called magnetization parameter  $\sigma$ , which is the ratio of the magnetic energy to kinetic energy of the unshocked flow, is smaller than unity, although the formation of the kinetic energy dominated flow within  $r \sim 10^{10-11}$  cm from the MSP is still of matter of debate (Lyubarsky & Kirk 2001). The magnetic field upstream and behind the shock are estimated as  $B_1(r) = (L_{sd}\sigma/r^2 c)^{1/2}$  and  $B_2(r_s) = 3B_1(r_s)$ , respectively. We assume a power law distribution of the accelerated particles at the shock,

that is,  $f(\Gamma) \propto \Gamma^{-p}$  for  $\Gamma_{min} \leq \Gamma \leq \Gamma_{max}$ . The photon index in the 0.5-10 keV band is observed as  $\alpha \sim 2$  for PSR B1957+20 (Huang & Becker 2007) and  $\alpha = 1.4 - 2$  for SAX J1808.4-3658 (Heinke et al. 2009), implying a power law index  $p = 1.8 - 3$ , which is found in the range predicted by the shock acceleration model (Baring 2004). We assume that the minimum Lorentz factor is comparable to the Lorentz factor of the bulk motion of the un-shocked flow, which is  $\Gamma_{min} \sim 10^5$  for  $\sigma \ll 1$  (Takata & Taam 2009). We determine the maximum Lorentz factor of the accelerated particles as  $\Gamma_{max} = \text{Min}(\Gamma_{syn}, \Gamma_g)$ , where  $\Gamma_{syn}$  is the Lorentz factor at which the synchrotron cooling time scale  $\tau_s \sim 9m_e^3 c^5 / 4e^4 B^2 \Gamma$  is equal to the acceleration time scale,  $\tau_{acc} \sim \Gamma m_e c / e B_2$ , that is,  $\Gamma_{syn} \sim 5 \times 10^7 L_{sd,34}^{-1/4} \sigma_{0.1}^{-1/4} r_{s,11}^{1/2}$ , where  $L_{sd,34} = (L_{sd}/10^{34} \text{ erg s}^{-1})$ ,  $\sigma_{0.1} = (\sigma/0.1)$  and  $r_{s,11} = (r_s/10^{11} \text{ cm})$ . In addition,  $\Gamma_g$  is the Lorentz factor at which the gyroradius is equal to the size of the system ( $\sim r_s$ ), that is,  $\Gamma_g \sim 3 \times 10^8 L_{sd,34}^{1/2} \sigma_{0.1}^{1/2}$ . The synchrotron spectrum extends from  $E_{min} \sim 260 L_{sd,34}^{1/2} \sigma_{0.1}^{1/2} r_{s,11}^{-1} \text{ eV}$  to soft- $\gamma$ -ray bands  $E_{max} \sim 2m_e c^2 \sin \theta / 8\alpha_f \sim 200 \text{ MeV}$  if  $\Gamma_{max} = \Gamma_{syn}$ , where  $\alpha_f$  is the fine structure constant, and  $E_{max} \sim 35 L_{sd,34}^{3/2} \sigma_{0.1}^{3/2} r_{s,11}^{-1} \text{ GeV}$  if  $\Gamma_{max} = \Gamma_g$ .

The steady continuity equation,  $\partial \dot{\Gamma} N_{tot}(\Gamma) / \partial \Gamma = \dot{Q}$ , implies that the distribution of the total number within the radiation cavity is expressed as  $N_{tot}(\Gamma) \propto \Gamma^{-p}$  for  $\Gamma_{min} \leq \Gamma \leq \Gamma_c$  in the slow cooling regime and  $N_{tot}(\Gamma) \propto \Gamma^{-1-p}$  for  $\Gamma_c \leq \Gamma \leq \Gamma_{max}$  in the fast cooling regime, where  $\Gamma_c$  is the Lorentz factor at which the synchrotron cooling scale  $\tau_s$  is equal to the dynamical time scale  $\tau_d \sim r_s / c$  (see Kong et al. 2011). In addition, the normalization is determined from the energy conservation that  $\int \Gamma N(\Gamma) d\Gamma = \eta L_{sd} \tau_d / m_e c^2$  (Arons & Tavani 1993), where  $\eta$  is the solid angle that the pulsar wind is stopped by the injected material from the low mass star. For the case of PSR B1957+20, the eclipse of the pulsar ( $\sim 10$ -20% of the orbital period) suggests that the angle of the mass flow from the LMS measured from the pulsar is  $\theta_a \sim 0.2$ . If the pulsar wind is emitted spherically, then  $\eta \sim \pi \theta_a^2 / 4 \sim 0.03$ .

The photon index of the emission is characterized by  $\alpha = (p + 1)/2$  for  $E_{min} < E < E_c$  and by  $\alpha = (p + 2)/2$  for  $E_c < E < E_{max}$ , where  $E_c \sim 1.6 L_{sd,34}^{-3/2} \sigma_{0.1}^{-3/2} r_{s,11} \text{ MeV}$  is the characteristic photon energy emitted by the particles with the Lorentz factor  $\Gamma_c$ . The predicted luminosity in the  $E_1 < E < E_2$  energy band is obtained by

$$\begin{aligned} L_s(E_1 < E < E_2) &\sim \int_{\Gamma_{min}}^{\Gamma_{max}} \int_{E_1}^{E_2} N_{tot} P_{syn} dE d\Gamma \\ &\sim 2 \times 10^{30} \left( \frac{\eta}{0.03} \right) \left( \frac{\Gamma_c}{10^5} \right) L_{sd,34}^2 \sigma_{0.1}^2 r_{s,11}^{-1} Q \text{ erg s}^{-1} \text{ for } p > 1, \end{aligned} \quad (49)$$

where  $P_{syn}$  is the synchrotron power per unit energy. In addition, the factor  $Q$  is expressed as

$$Q = (1 - p)(2 - p) \frac{[\int_{\Gamma_{min}/\Gamma_c}^1 \Gamma'^{2-p} d\Gamma' + \int_1^{\Gamma_{max}/\Gamma_c} \Gamma'^{1-p} d\Gamma'] \int_{x_{min}}^{x_{max}} F(x) dx}{(1 - p)[1 - (\Gamma_{min}/\Gamma_c)^{2-p}] - (2 - p)[(\Gamma_{max}/\Gamma_c)^{1-p} - 1]}$$

where  $\Gamma' = \Gamma/\Gamma_{min}$  and  $x = E/E_s$  with  $E_s = 3h\Gamma^2 eB \sin \theta / 4\pi m_e c$ , and  $x_{min} = E_1/E_s$  and  $x_{max} = E_2/E_s$  and  $F(x) = x \int_x^\infty K_{5/3}(y) dy$  with  $K_{5/3}$  being the modified Bessel function of order 5/3.

For SAX J1808.4+3365, the spin down power is expected to be  $L_{sd} \geq 10^{34}$  erg s<sup>-1</sup> from the enhancement of the optical emissions, and the separation between two components is inferred as  $a_0 \sim 3 \times 10^{10}$  cm (Chakrabarty & Morgan, 1998). Assuming  $L_{sd} = 5 \times 10^{34}$  erg s<sup>-1</sup>, for example, we find that the expected X-ray luminosity in the 0.5-10 keV energy band from equation (49) can be consistent with the observation,  $L_X \sim 10^{31-32}$  erg s<sup>-1</sup> (Heinke et al. 2009), when the magnetization parameter is larger than  $\sigma \sim 10^{-2}$ .

For the black widow systems, the predicted luminosity (49) in the 0.5-10 keV and 0.1-10 GeV energy bands are summarized in the seventh and eighth columns in Table 3, respectively, where the first and the second values corresponds to the results for the power law index  $p = 1.5$  and  $p = 3$ , respectively. In addition, we assume the separation between two components (sixth column) as the shock distance ( $r_s$ ). In Table 3, we also present the  $\gamma$ -ray (ninth column) and X-ray (tenth column) luminosity predicted by the outer gap model controlled by the magnetic pair-creation process.

The predicted luminosity of the intra-binary shock emission depends on the power law index ( $p$ ) and magnetization parameter ( $\sigma$ ). In Table 3, we see that the  $\gamma$ -ray luminosity predicted by the intra-binary shock changes by at least two orders of magnitude with the power law index between  $p = 1.5$  and  $p = 3$ . This dependence of the  $\gamma$ -ray luminosity on the power law index is more sensitive than that for the X-ray luminosity, since the number of particles that emit GeV photons is very sensitive to the photon index, while most particles emit X-rays.

Figure 10 summarizes the dependence of the predicted luminosity of the shock emission in X-ray (solid line) and  $\gamma$ -ray (dashed line) bands on the magnetization parameter. Here, the results are for PSR B1957+20 and for the power law index of  $p \sim 2$ . For the X-ray bands, we can see in Figure 10 that the luminosity (solid line) decreases with decreasing magnetization parameter. This results from the fact that the X-rays are emitted by the particles in the slow cooling regime and because the magnetic field decreases with decreasing  $\sigma$ . In the 0.1-10 GeV band, the luminosity (dashed-line) is not sensitive to the magnetization parameter if  $\sigma > 10^{-3}$ . For  $\sigma > 10^{-3}$ , the  $\gamma$ -ray photons are emitted by both particles in the slow and fast cooling regimes. As the magnetization parameter decreases, the magnetic field decreases, while more particles remain in the slow cooling regime. Since the former and latter effects tend to decrease and to increases the emissivity, respectively, two effects compensate each other. Below  $\sigma \sim 10^{-3}$ , we can see in Figure 10 that the  $\gamma$ -ray luminosity quickly decreases with decreasing magnetization parameter. This is because the maximum Lorentz factor for

$\sigma < 10^{-3}$  is limited by  $\Gamma_g$ , at which the gyroradius is equal to size of the system, and because the spectral cut-off of the synchrotron radiation,  $E_{max} \sim 35 L_{34, sd}^{3/2} (\sigma/0.001)^{3/2} r_{s,11}^{-1}$  MeV, appears below 100 MeV.

For PSR B1957+20, the non-pulsed X-ray luminosity is observed with a luminosity level of  $L_X(0.3 - 10\text{keV}) \sim 2.2 \times 10^{31} \text{ erg s}^{-1}$  (Huang & Becker 2007), which can be explained by the intra-binary shock model if the magnetization parameter  $\sigma > 0.01$ . Guillemot et al. (2011) find that the X-ray emissions from PSR B1957+20 are composed of the pulsed and non-pulsed components, although detail spectral properties of the pulsed component is still unknown. Guillemot et al. (2011) also report the detection of the pulsed  $\gamma$ -ray radiation from PSR B1957+20 using the *Fermi* data, whose observed flux level implies the luminosity of order of  $L_\gamma \sim 1 \times 10^{34} (d/2 \text{ kpc})^2 (\Delta\Omega_\gamma/4\pi) \text{ erg s}^{-1}$  (also see Kerr et al. 2010; Ray & Saz Parkinson 2011). As Table 3 indicates, the predicted luminosity level of the outer gap model (ninth column in Table 3) is found to be consistent with the *Fermi* observations with a typical solid angle  $\Delta\Omega_\gamma \sim 3$ .

For other systems, Table 3 indicates that the magnitude of the the predicted luminosity by the intra-binary shock model lies below the results of the *Fermi* observations, unless the power law index  $p \sim 1.5$ . For the  $\gamma$ -ray luminosity of PSR J1810+17, the predictions of both the outer gap and intra-binary shock models lie below the observation, implying that the true spin down power may be larger than that assumed using the relation  $\mu_{26} = P_{-3}^{7/6}/3$ .

Due to the uncertainties of the magnetization parameter  $\sigma$  and the power law index  $p$ , it is difficult to discriminate between the intra-binary shock model and the outer gap model for the unresolved X-ray emission from the “black widow” pulsar, unless the pulsed period is detected in the data. In addition to the pulsation search, future observations may be able to discriminate between models. For example, a measurement of the spectral shape in soft/hard X-ray bands and  $\gamma$ -ray bands can discriminate the emission models. The synchrotron spectrum from the intra-binary shock will extend from  $E_{min} \sim 200 \text{ eV}$  to  $E_{max} \sim 200 \text{ MeV}$  with a break at  $E_c \sim 1.6 L_{sd,34}^{-3/2} \sigma_{0.1}^{-3/2} r_{s,11} \text{ MeV}$ , implying the observed spectrum can be fit by a single power law function in the soft/hard X-ray bands and by a large photon index above  $\sim 100 \text{ MeV}$ . For the outer gap model, on the other hand, the spectral break will appear at  $\sim \text{keV}$  corresponding to the synchrotron radiation from the secondary pairs, as was discussed in section 5, and at  $\sim \text{GeV}$  corresponding to the curvature radiation in the outer gap. The observed soft X-ray spectrum with a index  $\alpha \sim 2$ , such as the X-ray emission of PSR B1957+20 (Huang & Becker 2007), may support the intra-binary shock, although the possibility that the spectrum with a cut-off energy  $\sim \text{keV}$  predicted by the outer gap model can not be excluded.

Finally, we would like to remark that (i) many new Black Widow systems will be associ-

ated with the *Fermi* un-identified sources and (ii) those systems will exhibit an eclipse of the radio emission. First, because of the radio eclipse, it is likely that many Black Widow systems have been missed by the previous radio surveys with the shorter observations. On the other hand, the MSPs in the Black Widow systems are younger and have higher spin-down power. This indicates that the MSPs in the Black Widow systems have larger  $\gamma$ -ray luminosity,  $L_\gamma \sim f^3 L_{sd}$  [equation (5)], than ordinary MSPs. Accumulating data of the *Fermi* observation will enable us to detect the  $\gamma$ -ray emissions from the Black Widow systems. In particular, the population studies (e.g. Kaaret & Philip 1996; Faucher-Giguère & Loeb 2010; Takata et al. 2011a,b,c) have pointed out that unidentified MSPs will be associated with the  $\gamma$ -ray sources located at higher Galactic latitude; for example, Takata et al. (2011a,b,c) argued statistically that the distribution of the high galactic latitude of the MSPs of the *Fermi* un-identified sources that manifest the spectral properties similar to the pulsars can be explained by the distribution of the MSPs. Second, because the  $\gamma$ -ray emission from the outer gap is greater in the direction perpendicular to the spin axis, *Fermi* is more likely to discover a greater number of MSPs with the Earth viewing angle  $\sim 90^\circ$  measured from the rotation axis (Takata, et al. 2010b; Takata, et al.2011c). If the angular momentum transferred from the accreting matter to the neutron star in the accreting stage produces the pulsar’s spin axis perpendicular to the orbital plane, the  $\gamma$ -ray emissions from MSPs in Black Widow will be greater in the orbital plane. Hence, *Fermi* will find the Black Widow systems with the Earth viewing angle described by edge-on rather than by face-on with respect to the orbital plane. In such a case, a greater number of the *Fermi* Black Widow systems will reveal eclipses of the radio emissions by the matter ejected from the companion star.

## 7. Summary and conclusion

With the recent accumulation of evidence for non-thermal X-ray and  $\gamma$ -ray emissions from different evolutionary stages of MSPs, we have investigated the high-energy emission processes of isolated rotation powered MSPs and those in binary systems. To understand their observational properties, the high-energy emission associated with the outer gap accelerator and with the intra-binary shock in the binary system has been investigated.

For the  $\gamma$ -ray emitting MSPs, the polar cap region is heated by incoming particles accelerated in the outer gap. These particles emit  $\sim 100\text{MeV}$  photons near the stellar surface which irradiate the polar cap region, eventually impacting on the stellar surface. The former and latter heating processes are identified with the rim component characterized by  $(T_r, r_r) \sim (7 \times 10^5\text{K}, 1\text{km})$  and the core component  $(T_c, r_c) \sim (2 \times 10^6\text{K}, 0.1\text{km})$ , respectively. For the outer gap model, the emission properties are controlled by either the

photon-photon pair-creation process between X-rays from the heated polar cap and the  $\gamma$ -rays or the magnetic pair-creation near the stellar surface. It has been found, based on the statistical grounds, that the outer gap controlled by the magnetic pair-creation process near the stellar surface (Takata et al. 2010b) is preferable in explaining the possible correlations in  $L_\gamma$  vs.  $L_{sd}$  (or  $\tau$ ) and  $L_{n,X}$  vs.  $L_{sd}$ .

For the AMP in the quiescent state of LMXBs, the observed modulation of the optical emissions and/or the non-thermal X-ray emission suggests the presence of rotation powered activities during this state. The thermal X-ray emission at the neutron star surface resulting from deep crustal heating can control the gap and, hence, the  $\gamma$ -ray emission properties. We find that if the optical modulation originates from the irradiation of  $\gamma$ -rays from the outer gap, the observed amplitude can constrain the NS model. For example, the level of the inferred irradiation luminosity  $L_{irr} \sim 10^{34}$  erg s $^{-1}$  of SAX J1808.4-3658 suggests that the outer gap with a high-mass NS model is preferable. As argued by Takata et al. (2010a), the presence of the outer gap emission would be responsible for the transition of the system from the LMXB phase to the rotation powered MSP phase.

Finally, we have discussed the high-energy emission from an intra-binary shock in the black widow systems, which are frequently found from radio searches of *Fermi* unidentified sources. Within the context of the simple one-zone model, we calculate the synchrotron emission from the accelerated particles at the shock. For PSR B1957+20, the observed non-pulsed X-ray emission ( $L_X \sim 2.2 \times 10^{31}$  erg s $^{-1}$ ) can be explained by the intra-binary shock model if the magnetization parameter is  $\sigma > 0.01$ . In addition, it is found that the observed luminosity of the pulsed  $\gamma$ -ray emission from PSR B1957+20 can be explained by the outer gap model. On the other hand, the 0.1-10 GeV emissions from the intra-binary shock is several orders of magnitude smaller than that from the outer gap emission, unless the magnetization parameter and the power law index of the accelerated particles are  $\sigma \geq 10^{-3}$  and  $p \sim 1.5$ , respectively. For the other black widow systems detected from *Fermi* unidentified sources, the predicted luminosity from the intra-binary shock model is consistent with the *Fermi* observations only if the power law index  $p \sim 1.5$ . In addition to the pulse search, the origin of the high-energy emissions from black widow systems will be constrained by a measurement of the spectral shape by new studies in the soft/hard X-ray bands, for example, by the Astro-H satellite, (Takahashi et al. 2010) ) and/or by *Fermi*.

We thank A.H.Kong, C.Y.Hui, P.H.T.Tam, R.H.H.Huang, Lupin-C.C.Lin, M.Ruderman, and S.Shibata for the useful discussions. We express our appreciation to an anonymous referee for useful comments. J.T. and K.S.C. are supported by a GRF grant of Hong Kong Government under HKU700911P and R.E.T This are supported in part by the Theoretical Institute for Advanced Research in Astrophysics (TIARA) operated under the Academia



Sinica Institute of Astronomy & Astrophysics in Taipei, Taiwan.

## REFERENCES

- Abdo A.A. et al. 2011, ApJL, 736, 11
- Abdo A.A. et al. 2010a, ApJS, 187, 460
- Abdo A.A. et al. 2010b, ApJS, 188, 405
- Abdo A.A. et al. 2010c, ApJ, 708, 1426
- Abdo A.A. et al. 2010d, ApJ, 712, 957
- Abdo A.A. et al. 2009a, Sci., 325, 840
- Abdo A.A. et al. 2009b, Sci., 325, 848
- Abdo A.A. et al. 2009c, ApJ, 706, 1331
- Aliu, E. et al. 2008, Sci, 322, 1221
- Alpar, M.A., Cheng, A.F., Ruderman, M.A. & Shaham, J., 1982, Natur, 300, 728
- Aharonian, F., et al., 2009, A&A, 507, 389
- Arons J., 1983 ApJ, 266, 215
- Arons J., & Tavani, M., 1994, 403, 249
- Baring, M.G., 2004, NuPhS., 136, 198
- Bogdanov, S. & Grindlay, J.E., 2009, ApJ, 703, 1557
- Brown, E.F., Bildsten, L. & Rutledge, R.E. 1998, ApJL, 504, 95
- Burderi, L., Di Salvo, T., D’Antona, F., Robba, N.R., & Testa, V. 2003, A&A, 404, L43
- Campana, S., Colpi, M, Mereghetti, S., Stella, L., & Tavani, M. 1998, A&ARv, 8, 279
- Chakrabarty, D., Morgan, E.H., 1998, Natur, 394, 346
- Chen, K., Ruderman, M., & Zhu, T. 1998, ApJ, 493, 397
- Cheng, K. S., Taam, R.E., & Wang, W., 2006, ApJ, 641, 427



- Cheng, K. S., Ho, C., & Ruderman, M. 1986a, *ApJ*, 300, 500
- Cheng, K. S., Ho, C., & Ruderman, M. 1986b, *ApJ*, 300, 522
- Cheng, K. S., & Zhang, L., 1999, *ApJ*, 515 337
- Cheng, K. S., Ruderman, M., & Zhang, L., 2000, *APJ*, 537, 964
- Colpi, M., Geppert, U., Page, D., & Possenti, A. 2001, *ApJL*, 548, 175
- D’Avanzo, P., Campana, S., Casares, J., Covino, S., Israel, G.L., & Stella, L. 2009, *A&A*, 508, 297
- Daugherty J.K. & Harding, A.K. 1996, *ApJ*, 458, 278
- Daugherty J.K., Harding, A.K. 1982, *ApJ*, 252, 337
- Deloye, C. J., Heinke, C. O., Taam, R. E., & Jonker, P. G. 2008, *MNRAS*, 391, 1619
- Faucher-Giguère, C.-A., & Loeb, A. 2010, *J. Cosmol. Astropart. Phys.*, JCAP, 1, 5
- Frank, J., King, A., & Raine, D. 2002, *Accretion Power in Astrophysics* (Cambridge: Cambridge Univ. Press)
- Gudmundsson, E.H., Pethick, C.J. & Epstein, R.I. 1983, *ApJ*, 272, 286
- Guillemot, L., et al. 2011, *arXiv1110.1271*
- Haensel, P. & Zdunik, J.L. 2003, *A&AL*, 404, 33
- Haensel, P. & Zdunik, J.L. 1990, *A&A*, 227, 431
- Halpern, J.P. & Ruderman, M. 1993, *ApJ*, 415, 286
- Harding, A. K. & Muslimov, A.G. 2011, *ApJL*, 726, 10
- Harding, A.K., Stern, J.V.; Dyks, J., Frackowiak, M. 2008, *ApJ*, 680, 1378
- Harding, A. K., Usov, V.V., & Muslimov, A.G. 2005, *ApJ*, 622, 531
- Heinke, C.O., Cohn, H.N. & Lugger, P.M. 2009, *ApJ*, 692, 584
- Hirokuni K. 2008, *ApJL*, 688, 25
- Huang, H.H. & Becker, W., 2007, *A&AL*, 463, 5
- Kaaret, P., & Cottam, J., 1996, *ApJL*, 462, 35

- Jonker, P. G., Torres, M. A. P., & Steeghs, D. 2008, *ApJ*, 680, 615
- Kalapotharakos, C., Kazanas, D., Harding, A., & Contopoulos, I., 2011, arXiv1108.2138
- Kargaltsev, O.Y., Pavlov, G.G., Zavlin, V.E. & Romani, R.W., 2005, *ApJ*, 625, 307
- Keith, M.J. et al. 2011, *MNRAS*, 414, 1292
- Kerr, M., Fermi LAT Collaboration, & Pulsar Timing Consortium. 2010, in *AAS/High Energy Astrophysics Division Meeting*, Vol. 11, 23.03
- Kong, S.W., Yu, Y.W., Huang, Y.F. & Cheng, K. S., 2011, *MNRAS*, 416, 1067
- Lang K.R. 1999, *Astrophysical Formulae* (New York: Springer)
- Lyubarsky, Y., & Kirk, J.G., 2001, *ApJL*, 547, 437
- Marelli, M., De Luca, A., & Caraveo, P.A., 2011, *ApJ*, 733, 82
- Muslimov, A.G. & Harding, A.K. *ApJ*, 617, 471
- Ray, P. & Saz Parkinson, P.M., 2011, in Rea N., Torres D. F., eds, *High-Energy Emission from Pulsars and Their Systems*. Springer, Berlin, p. 37
- Roberts, et al., 2011, to appear in *AIP Conference Proceedings of Pulsar Conference 2010 "Radio Pulsars: a key to unlock the secrets of the Universe"*, Sardinia, October 2010 (arXiv:1103.0819)
- Ruderman M. 1991, *ApJ*, 366, 261
- Ruderman M.A., Sutherland P.G. 1975, *ApJ*, 196, 51
- Romanova, M.M., Ustyugova, G.V., Koldoba, A.V., & Lovelace, R.V.E. 2009, *MNRAS*, 399, 1802
- Saz Parkinson, P.M. et al. 2010, 725, 571
- Spitkovsky A., 2006, 648, 51
- Stappers, B.W., Gaensler, B.M., Kaspi, V.M., van der Klis, M., & Lewin, W.H.G., 2003, *Sci*, 299, 1372
- Takahashi, et al.. 2010. *Proceedings of the SPIE*, 7732, 77320Z-77320Z-18
- Takata, J., Wang, Y., Cheng, K.S. 2011a, *ApJ*, 726, 44

- Takata, J., Wang, Y., Cheng, K.S. 2011b, MNRAS, 414, 2173
- Takata, J., Wang, Y., Cheng, K.S. 2011c, MNRAS, 415, 1827
- Takata, J., Cheng, K.S., Taam, R.E. 2010a, ApJL, 723, 68
- Takata, J., Wang, Y., Cheng, K.S. 2010b, ApJ, 715, 1318
- Takata, J., & Taam, R.E., 2009, ApJ, 702, 100
- Takata, J., Chang, H.-K. & Shibata, S., 2008, MNRAS, 386, 748
- Tam, P.H.T., Huang, R.H.H., Takata, J., Hui, C.Y., Kong, A.K.H. & Cheng, K.S., 2011, ApJL, 736, 10
- Tam, P.H.T. et al. 2010, ApJL, 724, 207
- Tavani, M., & Arons, J., 1997, ApJ, 477, 439
- Thorstensen, J. R., & Armstrong, E. 2005, AJ, 130, 759
- Venter C., Harding A.K., Guillemot L. 2009, ApJ, 707, 800
- Wada, T., & Shibata, S., 2011, MNRAS, in press
- Wang, F. Y.-H., Ruderman, M., Halpern, J.P. & Zhu, T., 1998, ApJ, 498, 373
- Wang, Y., Takata, J. & Cheng, K.S. 2010, ApJ, 720, 178
- Wang, Z., Archibald, A. M., Thorstensen, J. R., Kaspi, V. M., Lorimer, D. R., Stairs, I., & Ransom, S. M. 2009, ApJ, 703, 2017
- Webb, N. A., Olive, J.-F., Barret, D., Kramer, M., Cognard, I., Löhmer, O., 2004, A&A, 419, 269
- Webb, N.A., Olive, J.-F., Barret, D., 2004 A&A, 417, 181
- Yakovlev, D.G. & Pethick, C.J. 2004 ARA&A, 42, 169
- Yakovlev, D.G., Levenfish, K.P. & Haensel, P. 2003, A&A, 407, 265
- Zavlin, V.E. 2006, ApJ, 638, 951
- Zavlin, V.E. 2007, Ap& SS, 308, 297
- Zhang, L. & Cheng, K.S. 2003, A&A, 398, 639

Zhang, L. & Cheng, K.S. 1997, ApJ, 480, 370

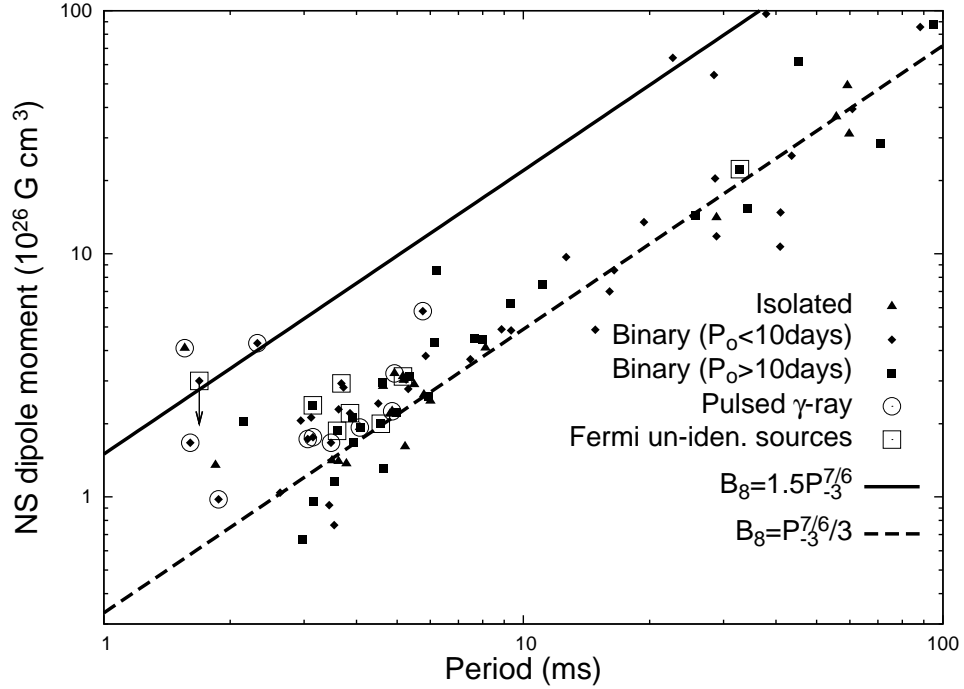


Fig. 1.— Spin period,  $P$ , vs.  $\mu$  for the rotation powered MSPs. The diamond with the vertical arrow represents the recently activated MSP, PSR J1023+0038 (Archibald et al. 2009). The open circles represent the  $\gamma$ -ray MSPs detected by the *Fermi*, and the open boxes represent the radio MSPs, whose positions are coincident with the *Fermi* unidentified sources. The data are taken from ATNF catalog (Manchester et al. 2005). The solid and the dashed lines correspond to the relation  $\mu_{26} = 1.5 P_{-3}^{7/6}$  and  $\mu_{26} = P_{-3}^{7/6} / 3$ , respectively (see text for details).

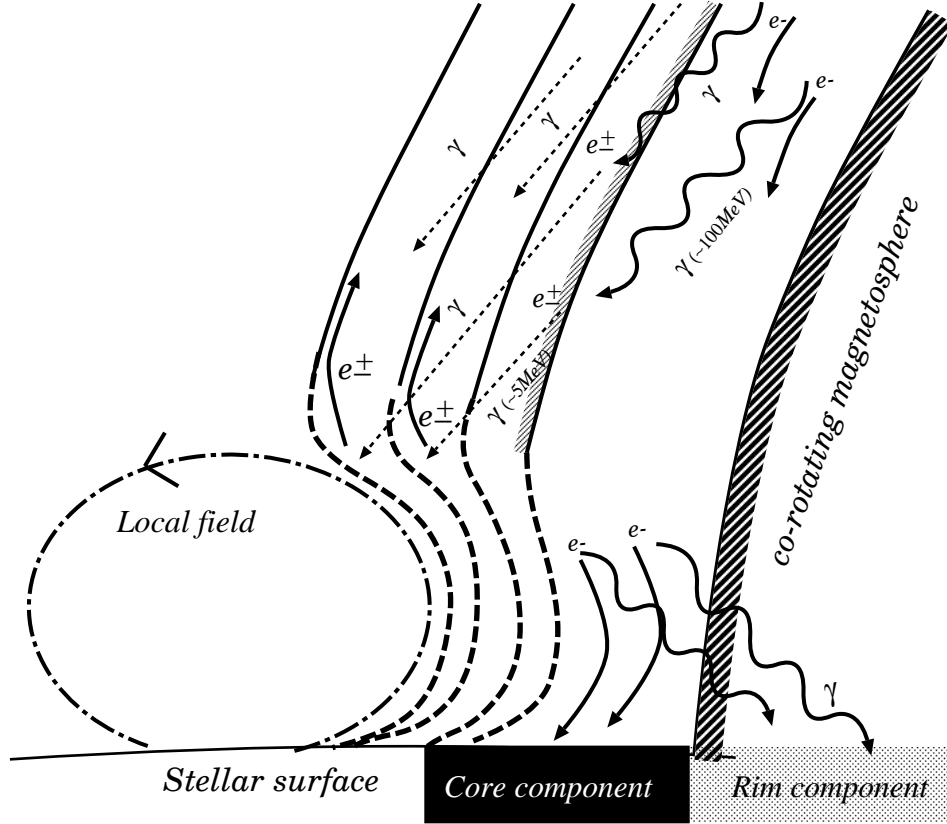


Fig. 2.— Schematic view for the structure of the polar cap region. Near the stellar surface, the multipole field components dominate the global dipole field, and the trajectory of the incoming particles and the emission direction of the  $\gamma$ -rays are determined by the local field. The rim component and core component are produced by the irradiation of the  $\gamma$ -rays between  $R_s \geq r \geq R_s + \delta R_{eq}$  and by bombardment of the incoming particles respectively.

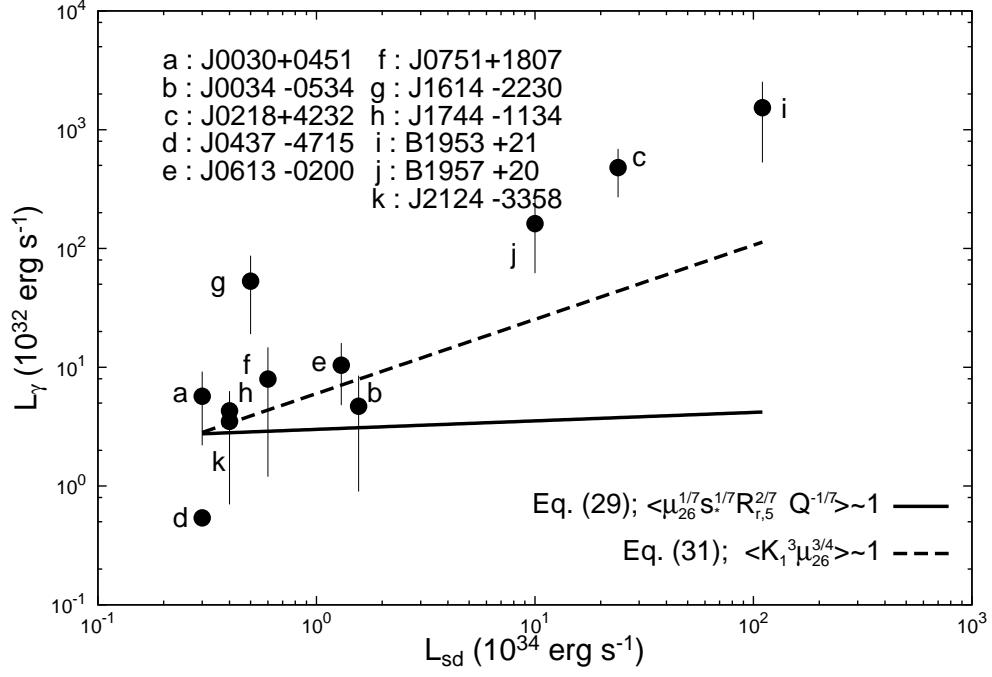


Fig. 3.—  $\gamma$ -ray luminosity,  $L_\gamma$  vs. spin down power,  $L_{sd}$ , for the rotation powered MSPs. The outer gap model controlled by the photon-photon pair-creation process between the  $\gamma$ -rays and X-rays from the heated polar cap (solid line) and by the magnetic pair-creation process near the stellar surface (dashed line) respectively. The data are taken from Abdo et al. (2010).



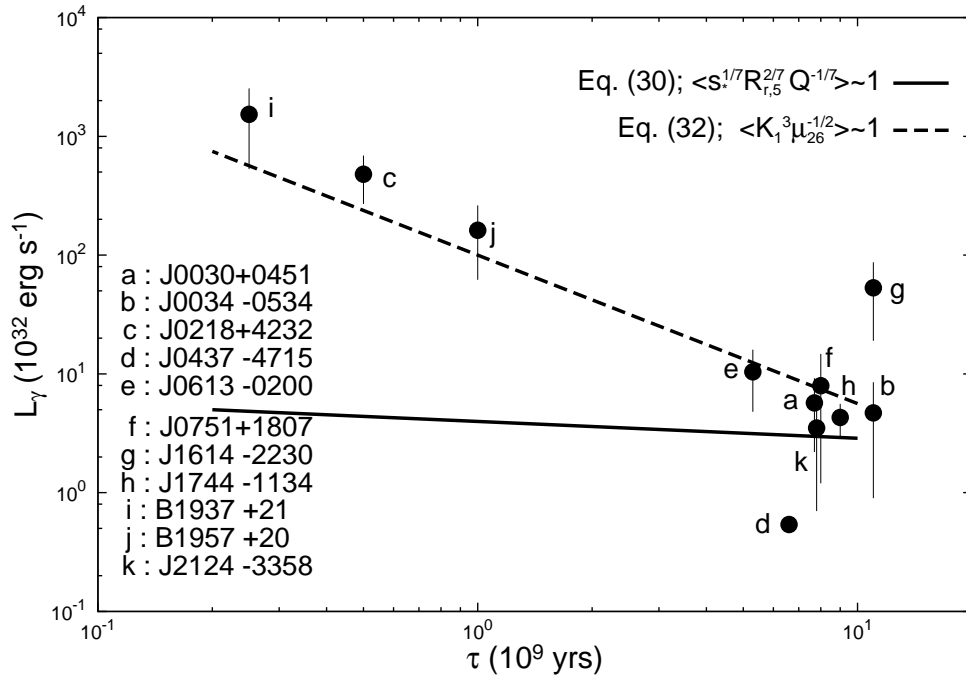


Fig. 4.—  $\gamma$ -ray luminosity,  $L_\gamma$ , vs. characteristic age. The lines and dots are same as Figure 3.

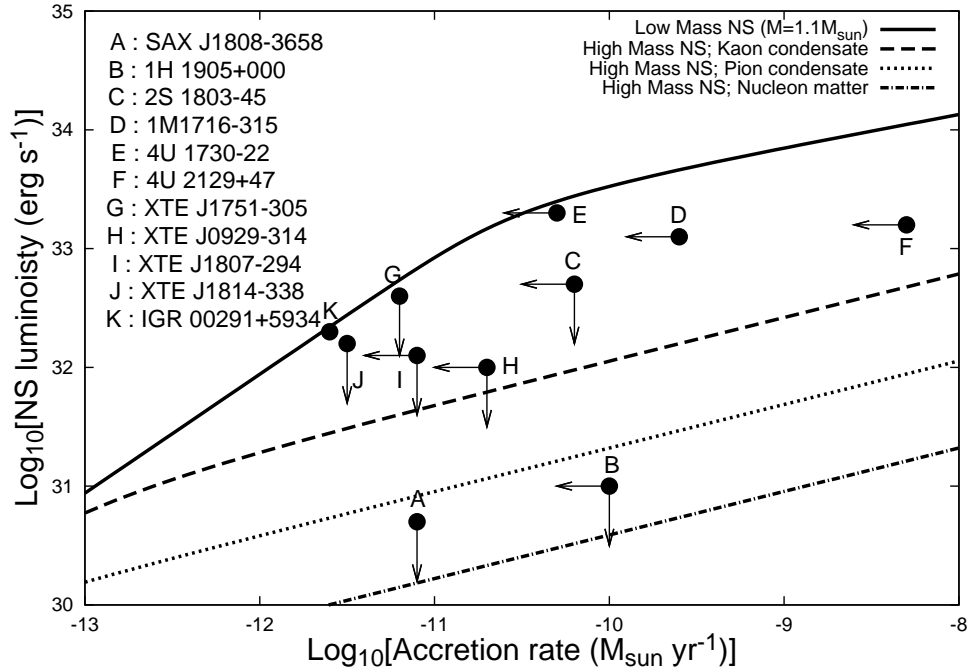


Fig. 5.— The quiescent thermal X-ray luminosity from the NS surface as a function of the averaged accretion rate. The predictions are for the low mass NS (solid line) and for various enhanced cooling mechanisms of the high mass NS (Yakovlev et al. 2003). The observational data are taken from Heinke et al. (2009).

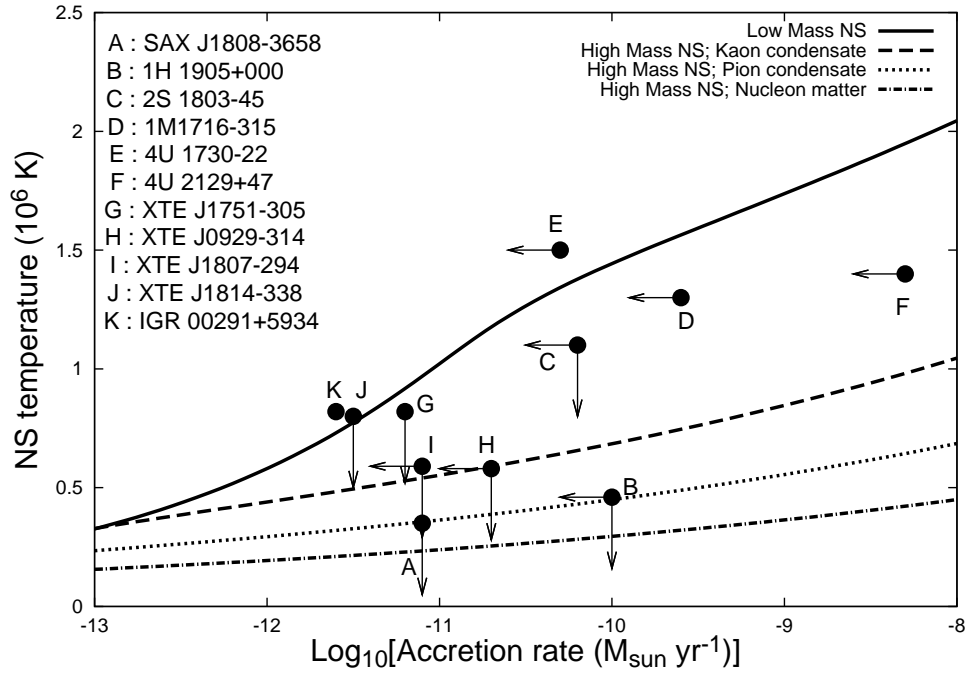


Fig. 6.— The surface temperature of the MSP in quiescent LMXBs as a function of the averaged accretion rate. The lines and dots are same as Figure 5.

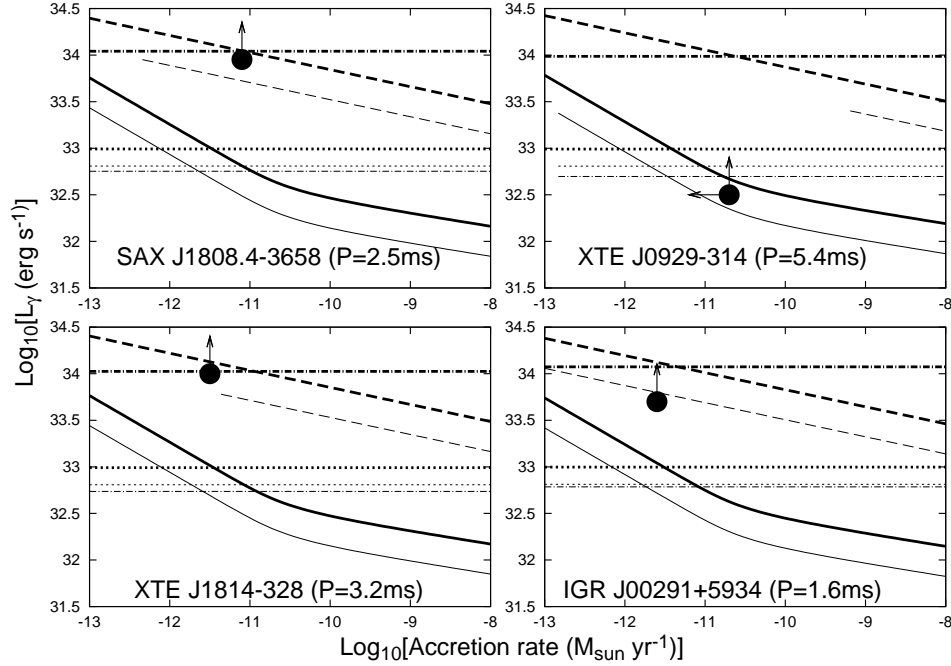


Fig. 7.— The predicted  $\gamma$ -ray luminosity as a function of the averaged accretion rate. The results for the outer gap controlled by photon-photon pair-creation between  $\gamma$ -rays and X-rays from full surface cooling emissions are represented by the solid line for low mass NS and by the dashed line for the high-mass NS with nucleon matter. In addition, the dotted line and dashed-dotted line represent results for the outer gap model controlled by the photon-photon pair-creation process between the  $\gamma$ -rays and X-rays from the heated polar cap and by the magnetic pair-creation process near the stellar surface, respectively. The thick and thin lines represent the magnetic field determined from  $\mu_{26} = P_{-3}^{7/6}/3$  and  $\mu_{26} = 1.5P_{-3}^{7/6}$ , respectively. In each line, the fractional gap thickness is limited below  $f \leq 1$ . The observational data (filled circles) represents the irradiating luminosity required to explain the optical modulation.

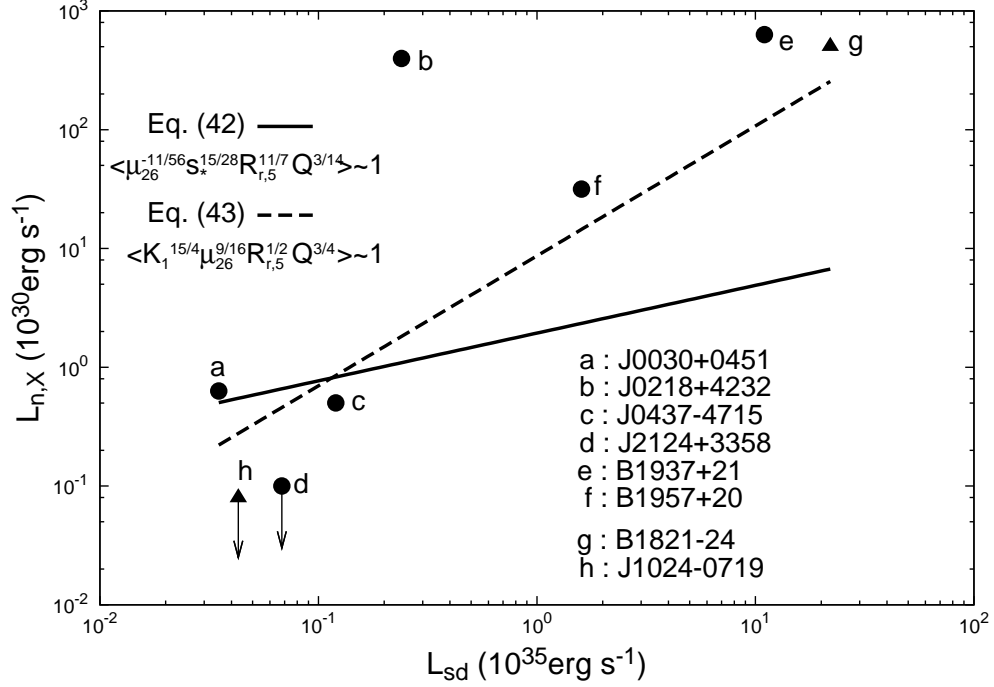


Fig. 8.— The non-thermal X-ray emission from the magnetosphere for the rotation powered MSPs. The solid and dashed lines represent the results for the outer gap model controlled by the photon-photon pair-creation process and by the magnetic pair-creation process. The filled circle and the triangles represent the  $\gamma$ -ray MSPs and radio MSPs respectively. The data are taken from Zavlin (2007).

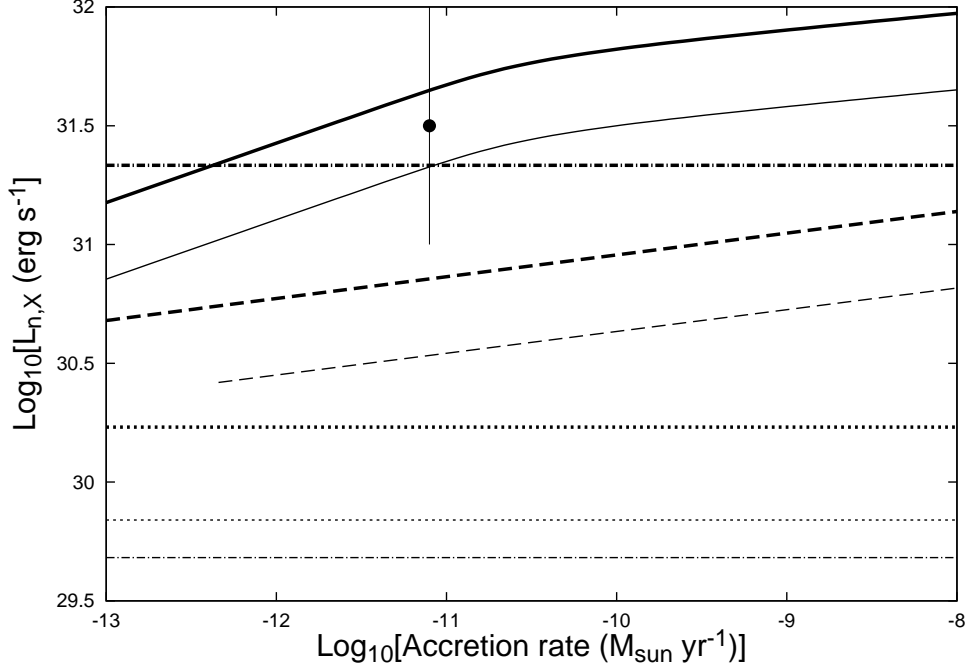


Fig. 9.— The pulsed non-thermal X-ray emission from the MSP in a quiescent LMXB. The solid and dashed lines represent the results for the outer gap models controlled by the photon-photon pair-creation process between the  $\gamma$ -rays and whole surface cooling X-ray emissions of a low mass NS and of a high-mass NS with nucleon matter and respectively. For comparison, the dotted line and dashed-dotted line represent results for the outer gap model controlled by the photon-photon pair-creation process between the  $\gamma$ -rays and X-rays from the heated polar cap and by the magnetic pair-creation process near the stellar surface, respectively. The thick and thin lines represent the magnetic field determined from  $\mu_{26} = P_{-3}^{7/6}/3$  and  $\mu_{26} = 1.5P_{-3}^{7/6}$  with  $P = 2.5$  ms, respectively. The filled circle represents the non-thermal emission from SAX J1808.4-3658 in quiescence.

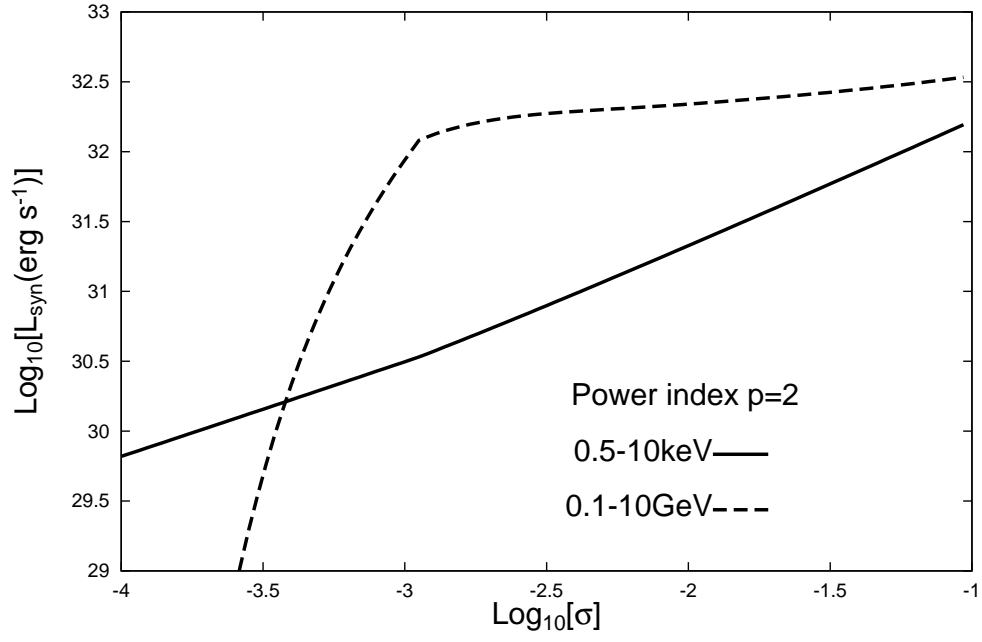


Fig. 10.— The luminosity vs. the magnetization parameter for the intra-binary shock model. The solid and dashed lines are the predicted luminosity for the 0.5-10 keV energy band and 0.1-10 GeV energy bands, respectively. The results are for the parameters of PSR B1957+20 and for a power law index corresponding to  $p \sim 2$ .

Pulsar name	$P$ (ms)	$\mu$ ( $10^{26}$ G cm <sup>3</sup> )	$\tau_c$ ( $10^9$ yrs)	$L_{sd}$ ( $10^{34}$ erg s <sup>-1</sup> )	$d$ (kpc)	$T_r$ ( $10^6$ K)	$R_r$ (km)	$T_c$ ( $10^6$ K)	$R_c$ (km)	$L_\gamma$ ( $10^{32}$ ergs <sup>-1</sup> )
J0030+0451	4.9	2.3	7	0.35	0.3	0.7	2	1.5	0.4 <sup>(a)</sup>	$5.7 \pm 3.5$
J0034-0534	1.9	0.7	11	2.9	0.53			2.2	0.05 <sup>(b)</sup>	$4.7 \pm 3.8$
J0218+4232	2.3	4.1	0.5	24.6	2.7			2.9	0.37 <sup>(c)</sup>	270-690
J0437-4715	5.8	3	6	0.29	0.156	0.52	2.9	1.4	0.39 <sup>(b)</sup>	$0.54 \pm 0.08$
J0613-0200	3.1	1.8	4	1.3	0.48					$8.9^{+7.1}_{-4.2}$
J0751+1807	3.5	1.5	8	0.7	0.62			3.7	0.04 <sup>(d)</sup>	$4.7^{+10}_{-3.5}$
J1614-2230	3.2	1.2	11	0.5	1.3			2.7	0.12 <sup>(e)</sup>	$53 \pm 34$
J1744-1134	4.1	1.8	8	0.4	0.47			3.2	0.03 <sup>(e)</sup>	$4.3 \pm 1.3$
B1937+21	1.6	4.1	0.2	110	7.7					560-2500
B1957+20	1.6	1.7	1	11	2.5					$\sim 100$
J2124-3358	4.9	2.4	6	0.4	0.25	0.5	1.8	2.2	0.1 <sup>(b)</sup>	$2.1^{+4.2}_{-1.4}$

Table 1: Observational properties of the millisecond pulsars detected by *Fermi*-LAT.  $P$ ; pulsar spin period,  $\mu$ ; magnetic moment of the neutron star,  $\tau_c$ ; spin down age,  $L_{sd}$ ; pulsar spin down power,  $d$ ; distance from the Earth,  $T_r$ ; surface temperature of the rim component,  $R_r$ ; effective radius of the rim component,  $T_c$ ; surface temperature of the core component,  $R_c$ ; effective radius of the core component and  $L_\gamma$ ;  $\gamma$ -ray luminosity. For the  $\gamma$ -ray luminosity, the data were taken from Abdo et al. (2009b). For the blanks in the columns  $T_r \sim R_c$ , no available data was found; (a) Bogdanov & Grindlay (2009), (b)Zavlin (2006), (c) Webb, Olive & Barret (2004), (d)Webb et al. (2004), and (e)Marelli, De Luca & Caraveo (2011).



Pulsar name	$T_r^{ob}$ ( $10^6$ K)	$T_c^{ob}$ ( $10^6$ K)	$L_\gamma^{ob}$ ( $10^{32}$ ergs $^{-1}$ )	$f_p$	$T_r^p$ ( $10^6$ K)	$T_c^p$ ( $10^6$ K)	$L_\gamma^p$ ( $10^{32}$ ergs $^{-1}$ )	$f_m$	$T_r^m$ ( $10^6$ K)	$T_c^m$ ( $10^6$ K)	$L_\gamma^m$ ( $10^{32}$ ergs $^{-1}$ )
J0030+0451	0.7	1.5	$5.7 \pm 3.5$	0.51	0.7	1.2	4.6	0.55	0.72	1.3	5.9
J0034-0534		2.2	$4.7 \pm 3.8$	0.37	0.55	3.8	6.5	0.34	0.56	3.6	5.8
J0218+4232		2.9	270-690	0.16	0.66	1.6	10	0.38	0.82	2.0	124
J0437-4715	0.52	1.4	$0.54 \pm 0.08$	0.60	0.6	1.2	6.5	0.60	0.6	1.2	6.6
J0613-0200			$8.9_{-4.2}^{+7.1}$	0.38	0.59	2.7	7.1	0.44	0.62	2.8	11.3
J0751+1807		3.7	$4.7_{-3.5}^{+10}$	0.48	0.5	4.0	6.5	0.47	0.57	3.9	5.8
J1614-2230		2.7	$53 \pm 34$	0.49	0.56	2.3	6.3	0.44	0.56	2.2	4.7
J1744-1134		3.2	$4.3 \pm 1.3$	0.53	0.58	4.6	6.5	0.50	0.58	4.4	5.7
B1937+21			560-2500	0.10	0.7	3.2	10	0.31	0.91	4.4	330
B1957+20			$\sim 100$	0.17	0.62	2.9	5.4	0.32	0.73	3.5	36
J2124-3358	0.5	2.2	$2.1_{-1.4}^{+4.2}$	0.48	0.73	2.4	4.3	0.55	0.76	2.5	6.4

Table 2: The X-ray and  $\gamma$ -ray emissions from rotation powered MSPs.  $T_r^i$  and  $T_c^i$  represent the temperatures of the rim and core components of the thermal X-ray emissions, respectively, and  $L_\gamma^i$  is the  $\gamma$ -ray luminosity. The superscript represents the observations ( $i = ob$ ), the predictions of the outer gap model controlled by the photon-photon pair-creation process ( $i = p$ ) and by the magnetic pair-creation process ( $i = m$ ), respectively. For the outer gap model controlled by the photon-photon pair-creation process ( $i = p$ ), the gap fraction ( $f_p$ ), the temperatures ( $T_r^p$ ,  $T_c^p$ ) and the luminosity ( $L_\gamma^p$ ) are calculated from equations (17), (21), (22), and (18), respectively, where we used (1) the observed effective radius if they were reported or (2) the typical value  $R_r = 3 \times 10^5$  cm and  $R_c = 10^4$  cm if there were no available observation results. In addition, we used the curvature radii corresponding to  $s_* = 0.5$ , and  $\zeta_6 = 1$ . For the outer gap model controlled by the magnetic pair-process  $i = m$ , the gap fraction  $f_m$ , the temperatures ( $T_r^m$ ,  $T_c^m$ ) and the luminosity ( $L_\gamma^m$ ) are calculated from equations (23), (27), (28) and (24), respectively, where we used  $K_1 = 1$ .

Pulsar name <sup>a</sup>	P (ms)	$L_{sd}$ $10^{34} \text{ erg s}^{-1}$	$L_{\gamma}^{ob}$ $10^{32} \text{ erg s}^{-1}$	$P_b$ hr	$a_o$ $R_{\odot}$	$L_{\gamma}^s$ $10^{32} \text{ erg s}^{-1}$	$L_X^s$ $10^{31} \text{ erg s}^{-1}$	$L_{\gamma}^m$ $10^{32} \text{ erg s}^{-1}$	$L_X^m$ $10^{31} \text{ erg s}^{-1}$
J0023+09(F)	3.05	0.66 <sup>†</sup>	8	3.3	1.3	0.5, 0.02	0.05, 0.23	5.5	0.04
J0610-21	3.86	0.23		6.9	2.1	0.1, 0.004	0.004, 0.02	2.7	0.01
J1731-1847	2.3	1.1 <sup>†</sup>		7.5	2.2	1, 0.003	0.09, 0.4	6	0.07
J1745+30(F)	2.65	1.3	19 <sup>‡</sup>	17.5	3.8	1, 0.003	0.09, 0.35	8.8	0.1
J1810+17(F)	1.66	1.8 <sup>†</sup>	120	3.6	1.3	2, 0.008	0.35, 1.5	6	0.1
B1957+20(F)	1.61	11	100	9.2	2.5	20, 0.05	9.3, 26	36	1
J2051-0827	4.51	0.53		2.4	1	3.9, 0.02	0.03, 0.2	8	0.05
J2214+30(F)	3.12	1.9	88	10.0	2.6	2, 0.006	0.2, 1	16	0.2
J2241-52(F)	2.19	3.3	10	3.4	1.3	4, 0.016	1.2, 4.4	17	0.3
J2256-1024(F)	2.29	5.2	4.3	5.1	1.7	7, 0.025	2.6, 8.6	28	0.5

Table 3: The predicted X-ray and  $\gamma$ -ray emissions from “black widow” MSPs. The MSPs associating with *Fermi* unidentified sources are denoted as (F) in the first column. The second ( $P$ ) and third ( $L_{sd}$ ) columns are the spin period and the spin down power of the pulsar, respectively; <sup>†</sup> we assumed  $\mu_{26} = P_{-3}^{7/6}/3$  (dashed-line in Figure 1) where the dipole moment of the neutron star has not been measured. The fourth column represents the expected  $\gamma$ -ray luminosity,  $L_{\gamma}^{ob} = 4\pi d^2 F_{>0.1}$ , where  $F_{>0.1}$  is the observed flux above 100 MeV, and  $d$  is the distance to the black widow system; <sup>‡</sup> we assumed  $d = 1$  kpc because of no available measurement. The fifth ( $P_o$ ) is the orbital period, and the sixth column ( $a_o$ ) is inferred separation (in units of the solar radius) of the two components if the Earth viewing angle is edge-on to the orbital plane. The seventh  $L_X^s$  and eighth  $L_{\gamma}^s$  columns represent the luminosity in the 0.5-10 keV and in 0.1-10 GeV energy bands, respectively, predicted by the intra-binary shock model [Eq. 49], where we assumed the shock distance  $r_s = a_o$ ,  $\eta = 0.03$  and  $\sigma = 0.1$ . In addition, the first and the second values shows the results for the power law index  $p = 1.5$  and  $p = 3$ , respectively. The ninth ( $L_{\gamma}^m$ ) and tenth ( $L_X^m$ ) column show the predicted  $\gamma$ -ray [Eq.(24)] and X-ray [Eq.(47)] radiations from the outer gap model controlled by the magnetic pair-creation model, respectively, where we assumed  $K_1 = 1$ ,  $R_{r,5} = 3$ , and  $\zeta_6 = 1$ .